Real-Time Measurements of a Bimolecular Reaction

by Christopher N Sipes

Submitted for the degree of
Master of Chemistry

The California Institute of Technology
August 16, 1988

Abstract

A method is described for the initiation of a bimolecular reaction with a laser. This allows the time resolution of bimolecular kinetics with ultrafast laser spectroscopy. Such kinetics are described for the case of $H + CO_2 \Rightarrow OH + CO$. The rise in OH is measured and examined via the proper intermediate-mediated kinetics -- the "biphasic" expression. The effect of restricting the impact parameter of the hydrogen atom on the carbon dioxide is also considered.

Introduction

Unimolecular decompositions are frequently studied in ultra-fast laser spectroscopy in order to understand chemical reaction dynamics.[1] Since most interesting chemical reactions involve two body collisions, unimolecular dissociations are analyzed as "half-collisions;" viewed in reverse they yield information on those multi-body collisions which are compleatly inelastic. While this technique has provided a wealth of knowledge, it does have its limitations. For instance, it is not well-adapted to studying reactions such as A + BC => AB + C which does not have a single-body product. This makes it difficult to understand the impact of transient intermediates, such as $[ABC]^{\dagger}$ above, on the course of a reaction. In this research report, I will describe a new technique utilised in the Zewail group to study such a reaction in real-time.

The bi-molecular reaction we set out to study is that of hydrogen atom with carbon dioxiode:

$$H + CO_2 => OH + CO.$$

The reverse reaction, that of hydroxyl radical with carbon monoxide, has been extensively studied.[2] Investigations of this reaction were motivated by its importance in both atmospheric chemistry -- as an important mechanism for hydroxyl radical removal -- and in combustion. The observed rate constant has been measured for a variety of temperatures and pressures -- not only of the reactants, but also of a neutral buffer gas

such as nitrogen or helium. The non-Arrhenius behavior of the kinetics, especially its dependence upon the pressure of neutral buffer gas, has led to the suggestion of a bound intermediate on the reaction path, as shown below:[2b]

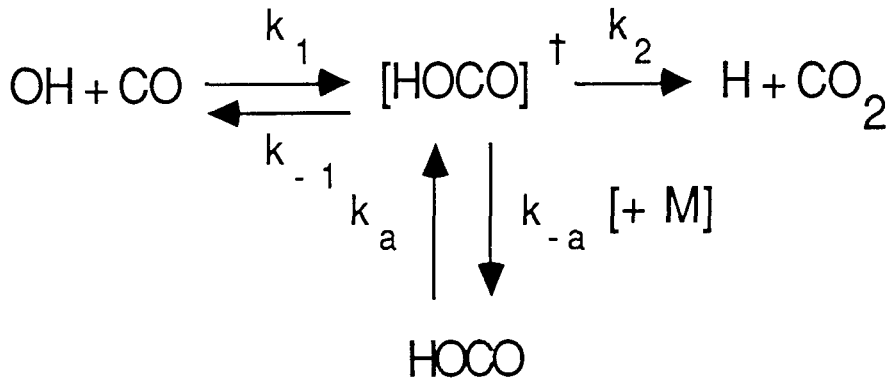

If we make the steady-state approximation for the excited intermediate $[HOCO]^{\dagger}$, we get:

$$0 = k_a[M][HOCO] + k_1[OH][CO] - k_{-1}[HOCO]^{\dagger} - k_2[HOCO]^{\dagger} - k_{-a}[M][HOCO]^{\dagger}$$

This can be rearranged to give:

$$[HOCO]^{\dagger} = \{k_a[M][HOCO] + k_1[OH][CO]\}/\{k_{-1} + k_2 + k_{-a}[M]\}$$

If the rate of formation of product is written as $k_{obs}[OH][CO]$, then we find:

$$k_{obs} = \{k_2k_1 + k_a[M][HOCO]/[OH][CO]\}/\{k_{-1} + k_2 + k_{-a}[M]\}$$

k_{obs} can be measured as a function of reactant and buffer gas pressure in order to extract the simple unimolecular and bimolecular rate constants (i.e., those describing steps with no bound intermediates along the reaction path). Using data measured by Hynes *et. al.*[2a], D.M. Golden and coworkers have done just that.[2a]

This forbidding task was greatly simplified. The proposed intermediate, HOCO, has been studied in matrix-trapping experiments.[3]

These have yielded a great deal of structural information as well as a force field. Using this force field, and treating the barrier height as a parameter, Golden performed a two-channel RRKM calculation to estimate the two unimolecular rate constants -- k_{-1} and k_2. Another simplification was a Lennard-Jones estimation of $k_{-a}[M]$. In this case, k_{-a} is rewritten as $\beta\omega$. β, which is between 0 and 1, is the collision efficiency, and ω is the collision rate. These were estimated from Lennard-Jones parameters and are dependent upon the nature of the buffer gas. Having estimated k_{-a} in this manner, k_a can be derived from the equilibrium constant K_1. Ultimately, the expressions were expressed as rate constants for:

$HOCO <=> OH + CO$	$k_{uni,1}(T,P)$ and $K_1(T)$
$HOCO <=> OH + CO_2$	$k_{uni,2}(T,P)$ and $K_2(T)$
$OH + CO => H + CO_2$	$k_{bi}(T,P)$

The temperature and pressure dependence of the above rate constants was not fit to an arbitrary functional form, however. The temperature dependence was fit to the modified Arrhenius expression $k = AT^b e^{-c/T}$. The pressure dependence was fit using the Troe formalism.[4]

Consider the two unimolecular decompositions shown above. In this case, write them as:

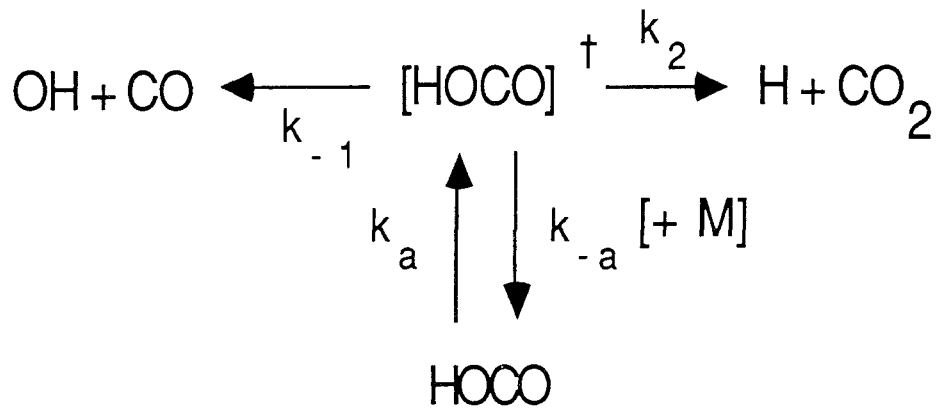

Again making a steady state approximation, we find:

$$[HOCO]^{\dagger} = k_a[HOCO][M]/(k_{-a}[M] + k_{-1} + k_2)$$

defing, as before, $\beta\omega = k_{-1}$, we can express the rate of carbon monoxide formation as:

$$k_{uni,1}[HOCO] = k_{-1}[HOCO]^{\dagger} = K_a\beta\omega k_{-1}[HOCO]/\{\beta\omega + (k_{-1} + k_2)/[M]\}.$$

Similarly, the rate of carbon dioxide formation is:

$$k_{uni,2}[HOCO] = k_2[HOCO]^{\dagger} = K_a\beta\omega k_2[HOCO]/\{\beta\omega + (k_{-1} + k_2)/[M]\}.$$

If we consider k_{uni} as a funtion of buffer gas pressure, we can take the high and low pressure limits and find:

$$\lim_{[M]=>\infty} k_{uni,1} = k_{uni,1}^{\infty} = K_a k_{-1}$$

$$\lim_{[M]=>0}(k_{uni,1})/[M] = (k_{uni,1}^{0})/[M] = K_a\beta\omega[k_{-1}/(k_{-1}+ k_2)]$$

$$\lim_{[M]=>\infty} k_{uni,2} = k_{uni,2}^{\infty} = K_a k_2$$

$$\lim_{[M]=>0}(k_{uni,1})/[M] = (k_{uni,1}^{0})/[M] = K_a\beta\omega[k_{-1}/(k_{-1}+ k_2)]$$

Golden *et. al.*[2b] fits the four rate constants $k_{uni,1}^{\infty}$, $(k_{uni,1}^{0})/[M]$, $k_{uni,2}^{\infty}$, and $(k_{uni,1}^{0})/[M]$ to the modified Arrhenius equation. We can use this to estimate the lifetime of the excited intermediate $[HOCO]^{\dagger}$ via each product channel as a function of temperature. To do this, we need to estimate the collision frequency (Golden's calculations were for air, which he corrected to be a strong collider -- $\beta = 1$).

Following Golden, we can use the Lennard-Jones collision rate Z:[5,2b]

$$Z = N_a\,\sigma^2\,(8RT/\pi\mu)^{1/2}\Omega^{2,2}$$

where:

N_a = Avogadro's number

σ = average L-J collision diameter = 4Å for HOCO-Air

μ = reduced collision mass = 17.6 g/mole for HOCO-Air

$\Omega^{2,2}$= L-J reduced collision integral, which can be approximated by the expression $[0.636 + 0.567\log(kT/\varepsilon)]^{-1}$ where ε is the L-J well depth = 200K for HOCO-Air

Plugging in, we find:

$$Z = (1.39\times10^{15}\ cm^3/mol\text{-}sec)(T/1000K)^{1/2}\Omega^{2,2}$$

Since, by assumption, $\beta = 1$, we get that $Z = \beta\omega$ and then, from above:

$$K_a(T) = (k_{uni,1}{}^0 + k_{uni,2}{}^0)/[M]Z$$

$$k_{-1}(T) = k_{uni,1}{}^\infty/K_a$$

and $k_2(T) = k_{uni,2}{}^\infty/K_a$.

We can then invert $k_{-1}(T)$ and $k_2(T)$ to derive the lifetimes as a function of temperature. Golden gives:

$$(k_{uni,1}{}^0)/[M] = 10^{23.34}T^{-1.89}e^{-1775/T}cm^3/mol\text{-}s$$

$$(k_{uni,2}{}^0)/[M] = 10^{26.36}T^{-3.024}e^{-1765/T}cm^3/mol\text{-}s$$

$$k_{uni,1}{}^\infty = 10^{12.77}T^{0.53}e^{-1710/T}s^{-1}$$

$$k_{uni,2}{}^\infty = 10^{12.24}T^{0.307}e^{-1657/T}s^{-1}$$

Putting this all together, we get expressions for the lifetimes which are plotted in figure 1. Note that this suggests that the rate of decomposition of $[HOCO]^\dagger$ to OH + CO is much faster than to H + CO_2.

The system was also analyzed by I.W.M. Smith and coworkers[2c] using transition state theory. The calculation was fit to measurements of the rate of vibrational relaxation of OH by CO done by Smith *et. al.*[2c] The relaxation of OH(v=1) by CO is believed to proceed via formation of [HOCO]†, which then either decomposes to H + CO_2 or to OH(v=0) + CO. The latter back-decomposition is expected to yield primarily vibrationally unexcited hydroxyl radical since energy transfer within the complex should be very rapid. Using this information, they were able to estimate the barrier to decomposition of HOCO into OH + CO to be $280cm^{-1}$ over the products.

The plethora of gas-phase data available for this reaction has encouraged many groups to study it under state-to-state conditions in

order to investigate how the dynamics of the collision complex affects the formation of products.[6] In particular, the collision of hydrogen atom with carbon dioxide has been studied under crossed beam conditions. These studies measured the distribution of product states rather than the kinetics of product formation. For instance, both Wolfrum *et. al.*[6c] and Tiee *et. al.*[6b] probed the final rotational state distribution of the hydroxyl radical as a function of hydrogen atom kinetic energy. They observed a fairly broad distribution; for instance, Wolfrum observed substantial population in J_{OH}=4 through J_{OH}=15 at a collision energy of 60kcal/mole. It is tempting to ascribe the breadth of the product angular momentum distribution to a scrambling of energy in the HOCO intermediate; however it is also possible that it may also be due to averaging over the angle of incidence of the hydrogen and other impact parameters. In order to truly understand the impact of a long-lived intermediate upon the dynamics of a reaction it is necessary to eliminate this additional uncertainty. It was with this in mind that the "precursor-limited geometry" technique (PLG) was developed.

Precursor-Limited Geometry Studies

In PLG reactions, an appropriate van-der-Waals cluster is constructed in a supersonic expansion. This cluster is then dissociated via a laser which serves to initiate the reaction. Wittig and coworkers[7], in order to study the reaction of hydrogen atom with carbon dioxide, formed the BrH···OCO complex. The hydrogen-bromine bond is dissociated with a 193nm photon from an excimer laser. The hydrogen recoils into the carbon dioxide which, for some collisions, then goes on to produce hydroxyl radical and carbon monoxide. The OH photoproducts are probed via LIF from the $^2\Sigma \Rightarrow {}^2\Pi$ transition. By tuning the probe wavelength, they are able to measure the rotational distribution of the OH products.

These precursor-limited geometry studies are very different from

the crossed beam studies done earlier. Perhaps most profound is the simple fact that the technique enables laser chemists to initiate what look like bimolecular reactions. We have exploited this in order to study the state-to-state reaction kinetics in real time.

Another difference is that the PLG technique more narrowly defines the impact parameters for this reaction. Klemperer and coworkers[8] have studied the van-der-Waals clusters FH···OCO and ClH···OCO with infrared Stark spectroscopy . They found that both complexes were linear with the hydrogen between the halogen and the oxygen. By analogy, it seems reasonable to postulate a similar linear structure XH···OCO for all the halogen halide, carbon dioxide clusters. In that case, Wittig and coworkers are measuring the rotational distributions of products formed exclusively from end-on attack of hydrogen on carbon dioxide. In fact, work done by Schatz *et. al.*[9] suggests that the OH products which are ultimately formed in this manner originate primarily from end-on collision angles varying from 5 to 10°.

In fact, Wittig sees a different rotational distribution than in the previous crossed beam experiments.[7] He observes a distribution which peaks at lower J_{OH} for comparable energies. This suggests that the intermediate complex "remembers" how it was produced. Rather than just conserving total angular momentum and energy, the reaction somehow conserves knowledge of the angle of attack of the hydrogen atom; a HOCO complex formed from end-on attack is different from one formed via broadside attack, and this difference lasts for a time commensurate with that for its dissociation. Either the activated HOCO complex dissociates much faster than expected or, for some reason, the energy is inhibited from redistributing. In either case, this result demonstrates that the dynamics of the transient intermediate can have dramatic effects upon the formation of products.

A previous study in the Zewail group addressed the issue by measuring the rate of formation of hydroxyl photoproduct.[10] In that study, the complex IH···OCO was formed. The hydrogen iodide bond was broken with a 239nm, picosecond laser pulse, and the OH product was detected via LIF from the $Q_1(1)$ line of the $^2\Sigma \Rightarrow {}^2\Pi$ transition. The lifetime of the intermediate HOCO was estimated to be 5 - 15 picoseconds. In this paper, I report the extension of this work to a variety of dissociation energies and detection of several rotational states.

Experimental Details

The IH···OCO complex was obtained in a seeded molecular beam as described previously.[10] 2% HI and 4% CO_2 were expanded in ~1600Torr He. The beam was characterized via electron impact mass spectroscopy, using 15 - 50 eV electrons and a home built time-of-flight spectrometer. A typical mass spectrum is shown in figure 2. HI disproportionates on metallic surfaces to yield I_2, so iodine was trapped out at -15° just prior to the nozzle plenum. Overall, about 3% of the HI formed the desired cluster. Cluster formation was kept at this low level in order to ensure that no significant signal came from the unwanted $(HI)_2OCO$ complex.

A mode-locked Nd^{3+}/YAG laser was used to synchronously pump a dye laser with an intracavity two-plate birefringent filter. Using Rhodamine 6G laser dye and DQOCI saturable absorber in ethylene glycol, this produced a 616nm laser pulse about 2ps long and 3Å in spectral width. The temporal width of the pulse could be monitored with a spinning-block autocorrelator in order to ensure that temperature fluctuations in the room did not broaden the pulses.

The laser pulse was then amplified in a pulsed dye amplifier pumped by the second harmonic of a Q-switched Nd^{3+}/YAG laser. This four-stage

amplifier, using Rhodamine 640 and Cresyl Violet 670 in methanol, produced 20Hz pulses of 616nm with approximately 0.4mJ of energy and the original temporal width. 20% of this light was then passed through a variable delay line and doubled via a KDP crystal to produce 308nm light. This light, the "probe," was used to detect the OH photoproduct via LIF.

The remaining 80% of the light was tightly focused into a 2.5cm cell of nanopure water. This created a continuum pulse with a temporal width similar to that of the input pulse. With a grating, the desired wavelength was selected and passed through a three-stage amplifier pumped by the third harmonic of the Q-switched Nd^{3+}/YAG and employing the appropriate Coumarin dye. The output was 50 - 100μJ pulses with about 7Å spectral width. The light was then doubled in a ß-BBO crystal to produce the pump wavelength. Since the pump wavelength, which is used to dissociate the HI, is related to the probe wavelength only via the continuum generator, the two wavelengths could be tuned independently of each other. This allowed us not only to study the reaction at a variety of dissociation wavelengths but also to probe different rotational states of the product OH.

The technique used was picosecond pump-probe spectroscopy. The pump pulse, by breaking the hydrogen iodide bond, initiates the reaction and therefore defines the time-zero of the process. By stepping the variable delay line the probe pulse could be varied in time relative to the pump. The generated LIF signal was then proportional to the amount of hydroxyl radical present at the time determined by this delay line setting.

In order to deconvolute the system response and precisely determine time-zero, the direct dissociation of hydrogen peroxide was monitored. The light generation and optical arrangement was kept exactly the same; however, the pulsed nozzle was stopped and the chamber filled with around 150mTorr of H_2O_2. A pump photon excites peroxide to a directly

dissociative surface producing two OH fragments; these were then observed with the probe pulse. These system responses were taken before and after each transient. The use of peroxide in the chamber as a system response had several advantages. Since the experiment and response were taken in the same place, the relative delay of the pump and probe pulses for a given delay line setting was unaltered; time-zero for the experiment and response is unquestionably the same. Moreover, since peroxide has a finite dissociation time (~100fs), the estimated resolution of our system is, if anything, an underestimate.

The Kinematics of IH···OCO Reactive Scattering

In order to estimate the kinematics of the PLG reaction, it is necessary to know the structure of the initial complex. As mentioned above, we will assume a linear structure for IH···OCO in analogy to the work done by Klemperer and coworkers.[8] Similarly, we can estimate the the length of the hydrogen bond by extrapolating from his measurements. Doing so, we estimate an O-H distance of about 2.35Å. This gives an H-C distance of about 3.5Å. From this, we can estimate the amount of angular momentum in the HOCO complex.

The bond strength of HI is well-known, and Herzberg[11] gives $D_0^0(^1H^{127}I) = 24{,}650cm^{-1}$. A 235nm photon carries $42{,}550cm^{-1}$ of energy, so $17{,}900cm^{-1}$ are available to the hydrogen and iodine atoms. Assuming that no internal excitation of the atoms occur, then by conservation of momentum, the hydrogen atom will acquire more than 99% of the energy. This gives a recoil velocity of 200Å/ps.

If we assume that the hydrogen approaches the carbon dioxide at about 7.5° (Schatz suggests 5-10°)[8], then the orbital angular momentum will be mvr(sin7.5°). At an initial H-C distance of 3.5Å, this is 90amu-$Å^2$/ps. We can convert this to angular frequency in HOCO by estimating its moment of inertia. It seems reasonable to assume that

this angular momentum will be perpendicular to the plane of the HOCO since the H-O-C angle should lie in the plane defined by the I-C axis and the hydrogen recoil. Thus, we need the component of the inertia tensor perpendicular to the plane. This can be estimated from the matrix-trapping work[3] to be about 50amu-Å^2. Using the relation $L_z = \omega I_z$, we find that the above angular momentum correlates to 1.8rad/ps = 3.5ps/rev. By contrast, had the hydrogen atom approached at 90° to the radius vector, the complex would have had more than 7 times this angular velocity. This, in itself, may account for the cooler rotational distribution of products.

Kinetics

It is useful to consider at this point what sort of kinetics we would associate with the simple scheme $A \overset{k_1}{\Rightarrow} B \overset{k_2}{\Rightarrow} C$[12]. Integrating $d(A)/dt = -k_1 t$, we find:

$$(A) = (A)_0 e^{-k_1 t}.$$

Since $d(B)/dt = k_1(A) - k_2(B)$,

we can substitute in the expression for (A) to get

$$d(B)/dt = k_1(A)_0 e^{-k_1 t} - k_2(B)$$

multiplying by $\exp(-k_2 t)$ and integrating, we find that

$$(B) = [k_1/(k_2-k_1)](A)_0 e^{-k_1 t} + Ce^{-k_2 t}.$$

For the condition $(B)_0 = 0$, we find that

$$(B) = [k_1/(k_2-k_1)](A)_0 [e^{-k_1 t} - e^{-k_2 t}].$$

Since, for $(C)_0 = 0$, $(C) = (A)_0 - (A) - (B)$, we then get that

$$(C) = (A)_0 \{1 + [k_2/(k_1 - k_2)]e^{-k_1 t} - [k_1/(k_1 - k_2)]e^{-k_2 t}\}.$$

In order to better appreciate this complicated expression, it is useful to find the delay from time-zero that the point of inflection of (C) occurs.

This period of induction is characteristic of a mechanism with an intermediate. To find the point of inflection of a function, we need to find a critical point whose second derivative is also zero; i.e., $d^2(C)/dt^2 = 0$ at p. However, since $d(C)/dt = -k_2(B)$, $d^2(C)/dt^2 = -k_2 d(B)/dt = 0$ at p. The point of inflection of (C) occurs at the same time that (B) reaches a maximum. The apparent delay in the observation of (C) is due to the lag in formation of the intermediate. Performing the necessary algebra, we find that this induction period, Δ, is $\ln(k_2/k_1)/(k_2 - k_1)$. This is very useful spectroscopically. If k_1 is much larger than k_2, then the observed risetime will be approximately k_1. However, this rise will be delayed by Δ from time zero. For instance, if k_1 is three times k_2, then Δ is still greater than one and a half times τ_1.

In the derivation of (B) above, the expression "$\exp(-k_1 + k_2)$" was integrated to yield "$k_1 - k_2$" in the denominator. This is only valid if k_1 is not equal to k_2. In that case, we find

$$(B) = (A)_0 k_1 t e^{-k_1 t}.$$

Once again using $(C) = (A)_0 - (A) - (B)$, we get the expression

$$(C) = (A)_0[1 - e^{-kt} - kte^{-kt}]$$

where $k=k_1=k_2$. In cases where the difference between k_1 and k_2 is smaller than the resolution of the experiment, we will see the modified exponential rise detailed above rather than a biphasic rise.

Data and Fits

Simply plotting the appropriate system response over each transient, an idea of the lag-time in product formation can be arrived at. This has been done in figures 3 and 4. These two transients both correspond to 235nm dissociation; in the first the $Q_1(1)$ transition was

probed and in the second the $Q_1(6)$ was. The relationship of each of the transients to their respective responses is clearly different. The hydroxyl product with small angular momentum is being produced later than that with high angular momentum. It is this effect which we seek to quantify with a biphasic fit.

We can fit both of the transients to the functional form:

$$(OH) \sim 1 + [k_2/(k_1 - k_2)]e^{-k_1 t} - [k_1/(k_1 - k_2)]e^{-k_2 t}.$$

The fits are shown in figures 5 and 6; the dashed line is the system response, the solid line corresponds to the fit. In the transient for the smaller J_{OH}, the fit yields two lifetimes; one of about 1.4ps and the other of about 2.3ps. This corresponds to a lag-time of around 1.8ps, which seems in accord with the shift between the transient and its response. Note that there is a degeneracy to the fit. The observed rise in (OH) is unaffected by permutting k_1 and k_2. Which lifetime corresponds to which step has to be argued on physical grounds, the fit does not say.

Fitting the $J_{OH} = 6$ transient, we get lifetimes equal to 1.546 and 1.547ps. This yields a lifetime of about 1.5ps. However, inspection of the transient and response do not reveal this large a shift. Moreover, the fact that $\tau_1 - \tau_2 \sim 0.001$ps makes the fit suspect since the coefficients have $k_1 - k_2$ in the denominator. Since our experimental resolution is much longer than 0.001ps, this suggests that we should use the modified exponential form with a single lifetime. The transients for 255, 243, 241, and 239nm dissociation, $Q_1(1)$ detection, and 235nm dissociation, $Q_1(6)$ detection, were all fit with the functional form:

$$(OH) \sim 1 - e^{-kt} - kte^{-kt}.$$

The results of these fits are shown in figures 7 - 12.

Thermodynamics

A potential energy surface for the reaction of hydrogen atom with carbon dioxide to yield carbon monoxide and hydroxyl radical has been calculated by Schatz and coworkers and is shown in figure 13. They estimate $\Delta H(H + CO_2 => t\text{-}HOCO) = 4{,}750cm^{-1}$. Since, as previously mentioned, the bond strength of hydrogen iodide is $24{,}650cm^{-1}$, this means that the total energy available to the HOCO complex is:

$$E_{max} = E_{h\nu} - 19{,}900cm^{-1}.$$

However, the HOCO complex may not acquire all of this energy. Both the channel giving $I_{1/2}$ and that giving $I_{3/2}$ carry oscillator strength. Thus, the dissociation of HI will be characterized by slow and fast hydrogen atoms, whose energy will differ by $7{,}000cm^{-1}$. For lower energy photons the slow channel should not produce much product, however, as the photon energy increases, we should begin to see products formed from both channels. Thus we will have two expressions for the internal energy in the HOCO intermediate, one for the fast hydrogens and one for the slow ones:

$$E_{fast} = E_{h\nu} - 19{,}900cm^{-1}$$

$$E_{slow} = E_{h\nu} - 26{,}900cm^{-1}$$

For lower energy photons, the slow channel should not produce much product, however, as the photon energy increases, we should begin to see products formed from both channels.

TABLE I[13]

Data for RRKM fit $[HOCO]^{\dagger}$ => OH + CO

HOCO:

frequencies of HOCO: 3456, 1833, 1260, 1077, 615, and 615 cm^{-1}

moments of inertia for HOCO: 49.7, 47.2, and 2.50 amu-$Å^2$

HO···CO Complex (bent):

frequencies of complex: 3456, 1900, 900, 425, and 175 cm^{-1}

moments of inertia for complex: 99.24, 95.66, and 3.58 amu-$Å^2$

barrier at 0K for complex: 13,250 cm^{-1}

Using the potential energy surface calculated by Schatz, the barrier calculated by I.W.M. Smith, and the critical configuration calculated by Golden, we can make an RRKM estimate for the rate of decomposition of HOCO into OH and CO as a function of energy. The parameters used are given in table 1 and the calculated lifetimes in figures 14 and 15. In particular, we estimate that below 250nm the fast channel produces a transient intermediate with a lifetime below 500femtoseconds. On the other hand, the calculation suggests a lifetime around 2.5ps for the slow channel at 235nm. Thus, hydroxyl radicals produced from each of these channels should be clearly distinguished from each other on the basis of lifetime.

Discussion of Results

The difference in the rate of formation of the $J_{OH} = 1$ fragment and the $J_{OH} = 6$ one is very interesting. Wittig saw a bimodal rotational distribution[7] which he attributed to the two spin-orbit states in bromine. We believe that we are seeing the same effect in our system; in fact, since the separation of the two states in iodine is 5000cm^{-1} larger than

in bromine, the effect should be even more pronounced. That is, the rotational distribution from the slow hydrogen channel will be weighted to much lower J_{OH} than from the fast. Hence, at 235nm dissociation, the hydroxyl fragments probed with the $Q_1(1)$ transition will be primarily produced via excitation to the I* channel while the $Q_1(6)$ transition will probe fragments produced along with ground-state iodine.

If our hypothesis is correct, it provides a convenient way to study the reaction at small excitation energy. The degree to which the pump energy can be reduced is limited by the HI absorption which drops off quickly to the red of 255nm.[14] However, by observing the products from the I* channel, we can shift the barrier 7,000cm^{-1} to the blue. With slow hydrogens, a 235nm pump wavelength produces $[HOCO]^{\dagger}$ only 2,400cm^{-1} over the barrier, compared to 6,400cm^{-1} over the barrier for the fast channel at 255nm. This will permit us to map out the kinetics over the whole range of excitation energies.

The lifetimes derived from the modified exponential fits are also very interesting since they are considerably longer than those predicted by the RRKM fit. It is possible that our resolution was not great enough to resolve faster lifetimes. However, we consider it also possible that the intermediate does in fact exist for a considerably longer period of time than predicted. One reason for this is that the $[HOCO]^{\dagger}$ complex actually has less energy than calculated above.

In the analysis above, we assumed that the hydrogen iodide dissociation is complete before the hydrogen impacts the carbon dioxide. If this is true, we are justified in assigning more than 99% of the energy to the hydrogen. When the H atom interacts with the CO_2, most of the energy remains as potential. The effect of this can be highlighted with the use of an extreme example.

If the hydrogen were to impact upon the carbon dioxide immediately after excitation and the carbon dioxide was to remain perfectly rigid, then the iodine would feel a recoil from the impact. As potential energy is converted into kinetic, the resulting momentum would be equally shared between the iodine and the [H+OCO] complex, which has 45/127ths the mass. In this case, the HOCO would only acquire 74% of the energy from the HI dissociation.

Of course, this approximation is rather extreme. When the hydrogen impacts the carbon dioxide, the CO_2 does not remain rigid. The potential energy is converted into deformation of the [H+OCO] complex to form HOCO and ultimately into vibrational excitation of HOCO itself. In a sense, deformation of the CO_2 serves to "cushion the blow;" converting potential into internal excitation of the HOCO and lessening the recoil of the iodine. Nevertheless, the HOCO complex will acquire some kinetic energy and, to the extent that it does, conservation of momentum will require that the iodine acquire a proportionate amount.

The amount of energy that the iodine actually acquires, and therefore the amount of kinetic and internal excitation of the HOCO complex, will probably be intermediate between the two cases examined above: the iodine will acquire more energy than if it recoiled from a bare hydrogen but less than recoil from a rigid HOCO. In fact, it may be that the division of energy will not be the same in every reactive collision. Depending upon the exact impact parameters, the amount of potential energy which is converted to vibrational excitation of HOCO will differ, and this amount will determine the amount of recoil the iodine feels. Hence, we may be probing the hydroxyl radicals formed from intermediates with a distribution of energies.

Future Work

Future work on this problem will be addressed towards answering

some of the uncertainties that remain. The first hypothesis we would like to examine is the possibility of the I* channel at 235nm. This can be examined by taking rotational state distributions at several pump wavelengths. By comparing the rotational state distribution of the hydroxyl radicals produced from 235nm excitation to that at 241nm or 255nm, we may be able to detect a bimodal distribution at high energy that then goes away as we tune to the red. This would be strong confirmation of our hypothesis. If in fact we are confirmed, it then seems interesting to tune the pump further to the blue. This will allow us to map out the kinetics at low energy.

We would also like to extend this work to the femtosecond domain. This will allow us to better examine the lifetime at high energy. In this case, we will have a much better set of data to compare to the RRKM fits. This may allow us to estimate the amount of kinetic energy that the iodine acquires as well as the nature of its energy distribution.

REFERENCES

(1) See, for example, R. D. Levine and R. B. Bernstein "Molecular Reaction Dynamics and Chemical Reactivity" Oxford University Press, New York, 1987.

(2) a) A. J. Hynes; P. H. Wine; and A. R. Ravishankara *J. Geophys. Res. D* **1986**, 91, 815.
b) C. W. Larson; P. H. Stewart; and D. M. Golden *Int. J. Chem. Kinetics* submitted for publication.
c) J. Brunning; D. W. Derbyshire; I. W. M. Smith; and M. D. Williams submitted for publication.

(3) D. E. Milligan and M. E. Jacox *J. Chem. Phys.* **1971**, 54, 927.

(4) J. Troe *Ber. Bunsenges Phys. Chem.* **1983**, 87, 161.

(5) J. O. Hirschfelder, C. F. Curtis, R. B. Bird "Molecular Theory of Gases and Liquids" John Wiley and Sons, New York, 1954.

(6) a) G. A. Oldershaw and D. A. Porter *Nature* **1969**, 223, 490.
b) C. R. Quick, Jr. and J. J. Tiee *Chem. Phys. Lett.* **1983**, 100, 223.
c) K. Kleinermanns and J. Wolfrum *Chem. Phys. Lett.* **1984**, 104, 157.

(7) a) S. Buelow; G. Radhakrishnan; J. Catanzarite; and C. Wittig *J. Chem. Phys.* **1985**, 83, 444.
b) G. Radhakrishnan; S. Buelow; and C. Wittig *J. Chem. Phys.* **1986**, 84, 727.
c) S. Buelow; *et. al. J. Phys. Chem.* **1986**, 90, 1015.
d) S. Buelow; G. Radhakrishnan; and C. Wittig *J. Chem. Phys.* **1987**, 91, 5409.

(8) a) F. A. Baiocchi; T. A. Dixon; C. H. Joyner; and W. Klemperer, *J. Chem. Phys.* **1981**,74,6544.
b) R. S. Altman; M. D. Marshall; and W. Klemperer *J. Chem. Phys.* **1982**, 77, 4344.

(9) a) G. C. Schatz; M. S. Fitzcharles; and L. B. Harding submitted for publication.
b) G. C. Schatz and M. S. Fitzcharles submitted for publication.

(10) N. F. Scherer; L. R. Khundkar; R. B. Bernstein; and A. H. Zewail *J. Chem. Phys.* **1987**, 87, 1451.

(11) G. Herzberg "Molecular Spectra and Molecular Structure" Van Nostrand Reinhold Company, New York, 1950, Vol. I, p.540.

(12) See, for example, J. H. Esperson "Chemical Kinetics and Reaction Mechanisms" McGraw Hill, New York, 1981.

(13) Frequencies and moments of inertia of HOCO and complex from reference 2b. HOCO frequencies were corrected to match reference 3. Barrier height taken from reference 2c.

(14) B. J. Huebert and R. M. Martin *J. Chem. Phys.* **1968**, 72, 3046.

FIGURE CAPTIONS

figure 1. Plot of lifetime versus Temperature calculated from the parameters given by Golden *et. al.*[2b] The open squares are for the reaction HOCO => H + CO_2, the closed ones for HOCO => OH + CO.

figure 2. Typical mass-spectrum of the supersonic expansion. Note that the deflection grids are optimized for HI. CO_2 to HI ratio is actually 2-1.

figures 3 and 4. Plots of hydroxyl rise times in dissociation of HOCO (solid line) and HOOH (dashed line). HOOH is system response as described in text.

figures 5 and 6. Same as above but including biphasic exponential fit.

figures 7 - 12. Plots of hydroxyl rise times from HOCO and HOOH for the wavelengths listed. The fits are for the modified exponential function $e^{-kt} + kte^{-kt}$.

figure 13. Diagram of potential energy surface as diagrammed by Schatz in reference 9.

figure 14. Plot of lifetime for the decomposition of $[HOCO]^{\dagger}$ to hydroxyl and carbon monoxide calculated via RRKM. Parameters that were used are listed in Table I. The top graph is versus wavelength of the pump photon assuming production of a ground-state iodine. The bottom graph assumes production of a spin-orbit excited iodine.

figure 15. a) Same RRKM calculation as for figure 14, now plotted as a function of HOCO internal energy.

b) Detail of figure 15a and including fits to experimental data. The fits are for 255, 243, 241, 239, and 237nm, $Q_1(1)$ detection, and 235nm, $Q_1(6)$ detection, as shown in figures 7 - 12. The $[HOCO]^{\dagger}$ internal energy was calculated assuming fast H's.

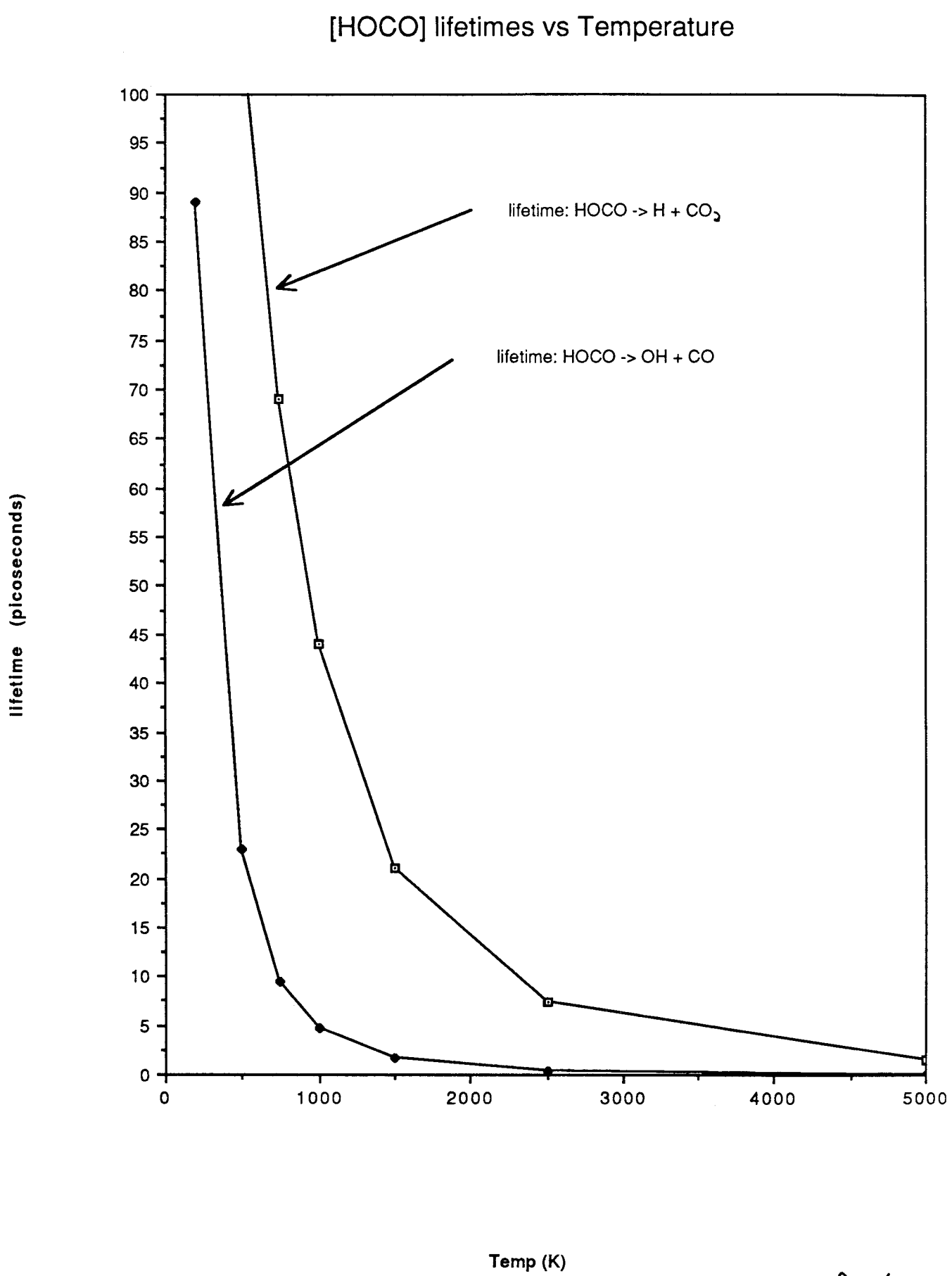
[HOCO] lifetimes vs Temperature
lifetime: HOCO -> H + CO2
lifetime: HOCO -> OH + CO
lifetime (picoseconds)
Temp (K)
0
5
10
15
20
25
30
35
40
45
50
55
60
65
70
75
80
85
90
95
100
0
1000
2000
3000
4000
5000

fig 1

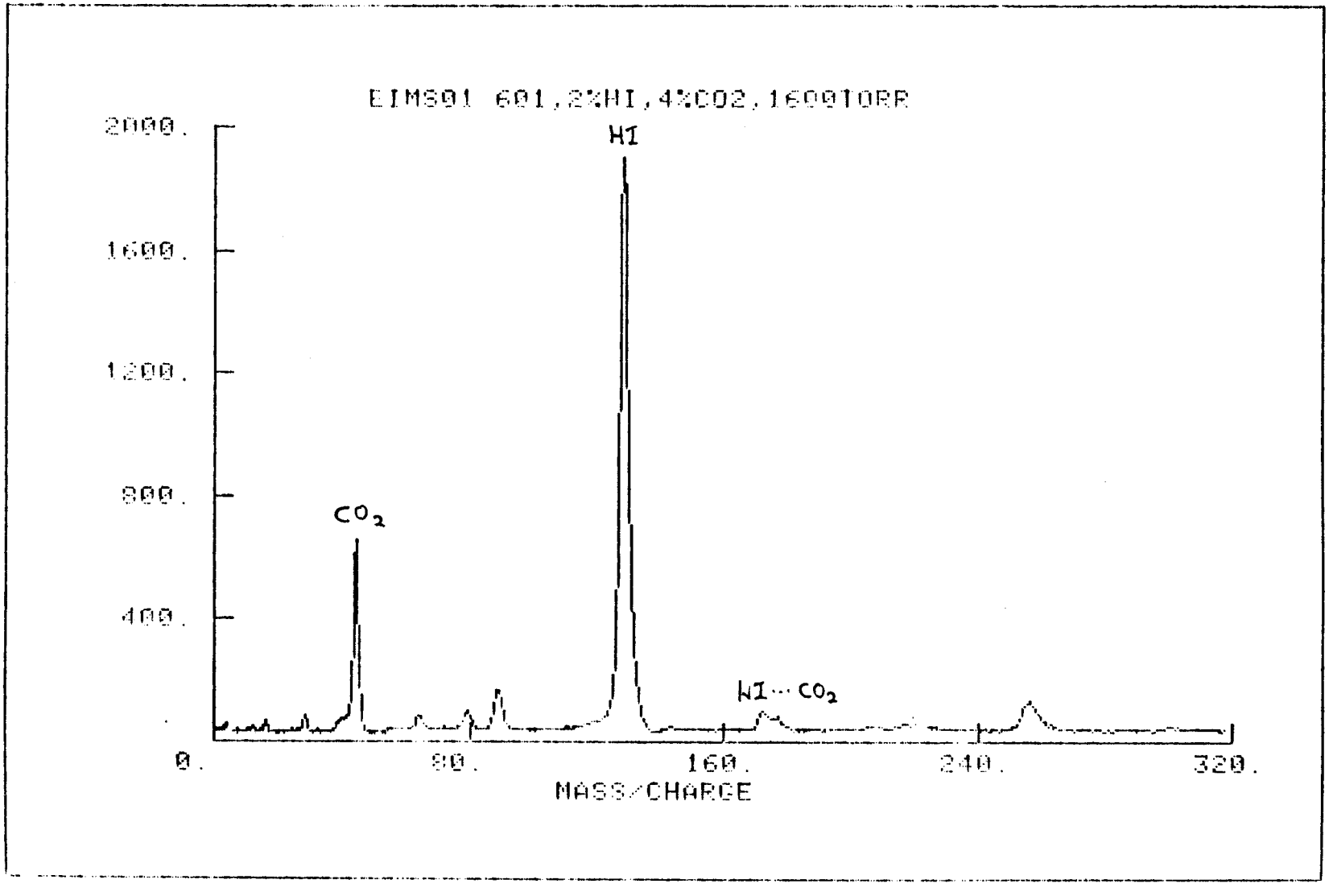
EIMS01 601,2%HI,4%CO2,1600TORR
2000.
1600.
1200.
800.
400.
0.
80.
160.
240.
320.
MASS/CHARGE
HI
CO_2
$HI\cdots CO_2$

Fig. 2

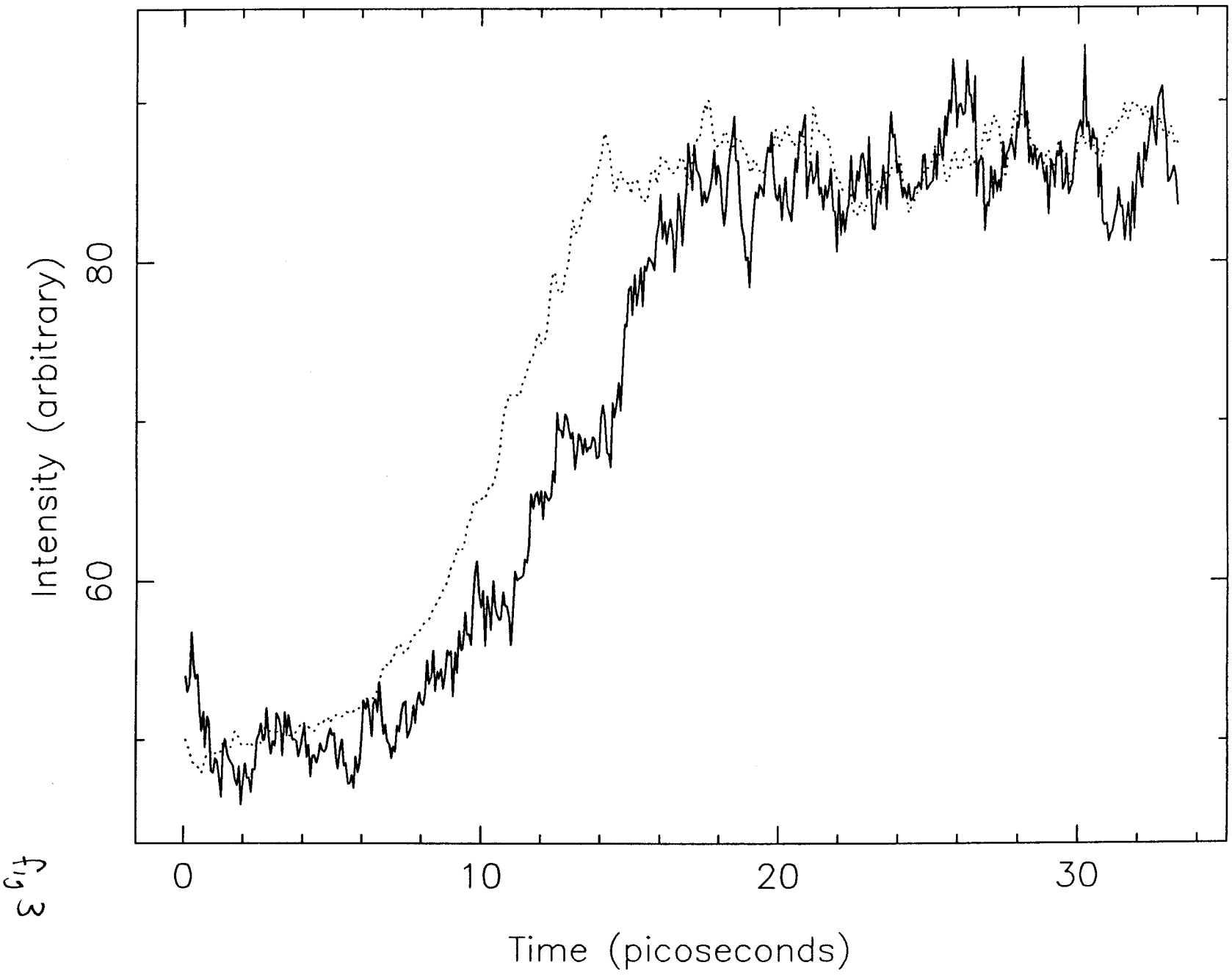
Pump = 235nm, probe OH ($Q_1(1)$)
Intensity (arbitrary)
60
80
0
10
20
30
Time (picoseconds)

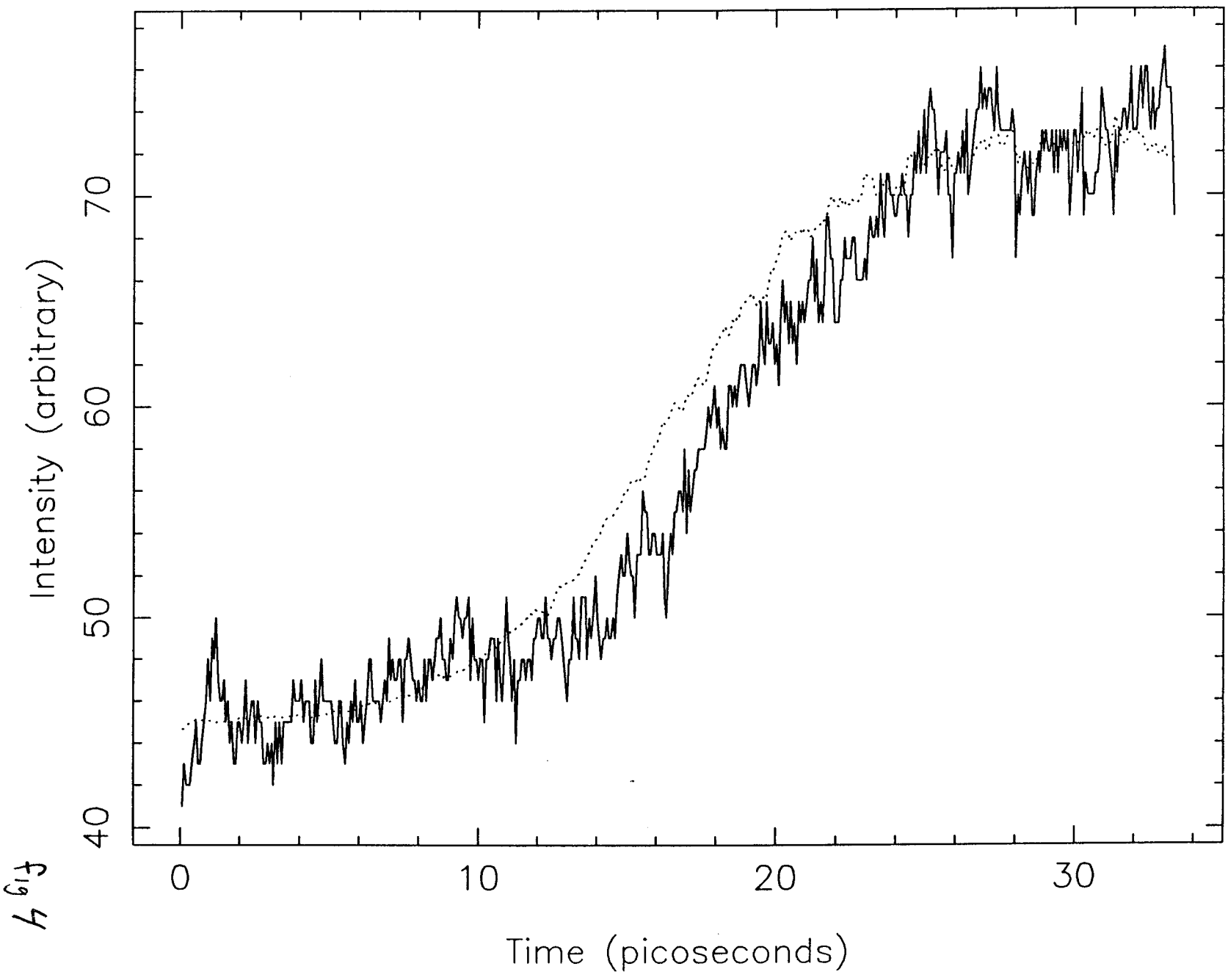
Pump = 235nm, probe OH ($Q_1(6)$)
Intensity (arbitrary)
40
50
60
70
0
10
20
30
Time (picoseconds)

Fig 4

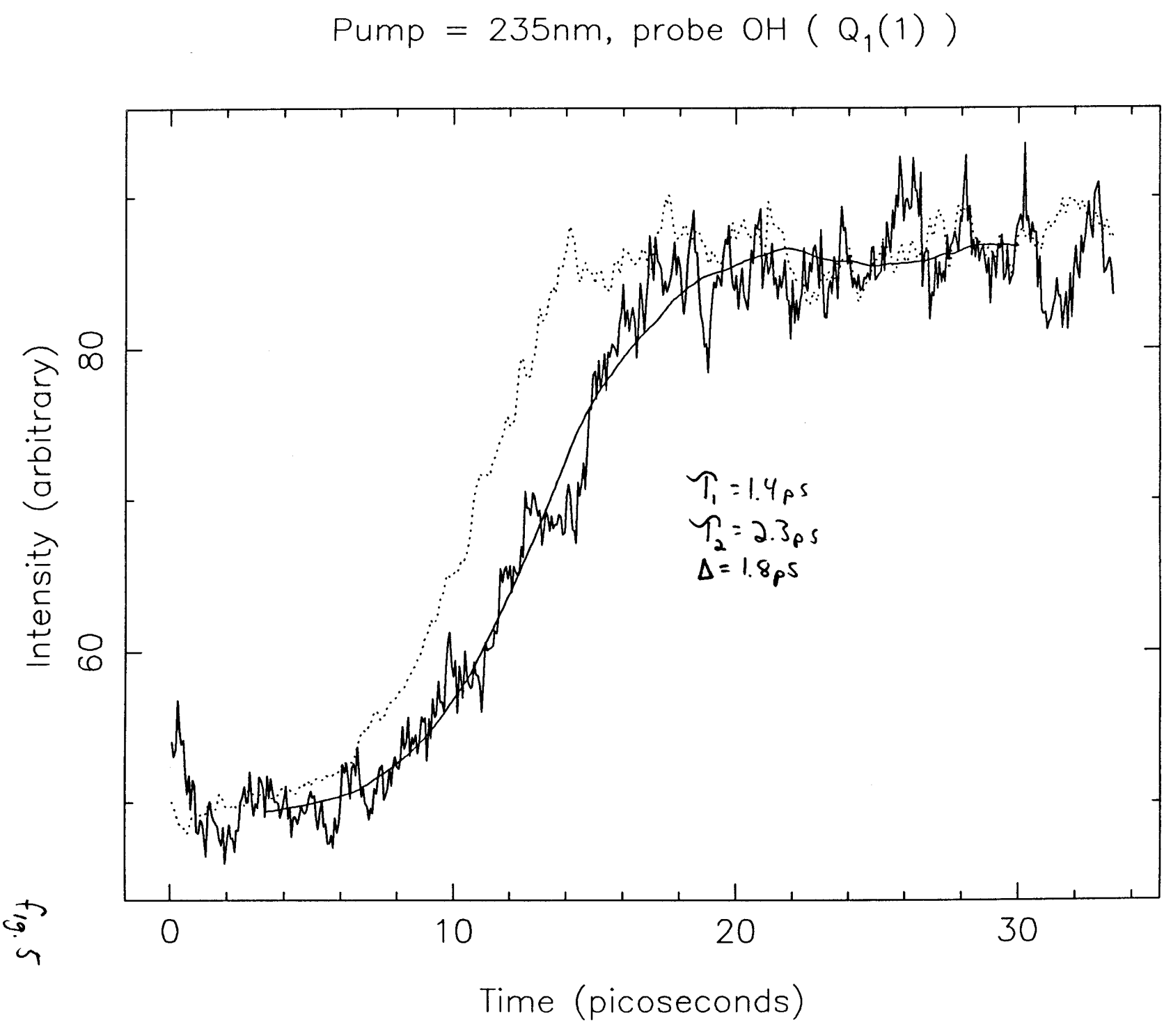
Pump = 235nm, probe OH ($Q_1(1)$)
Intensity (arbitrary)
60
80
0
10
20
30
Time (picoseconds)
$\tau_1 = 1.4$ ps
$\tau_2 = 2.3$ ps
$\Delta = 1.8$ ps
Fig. 5

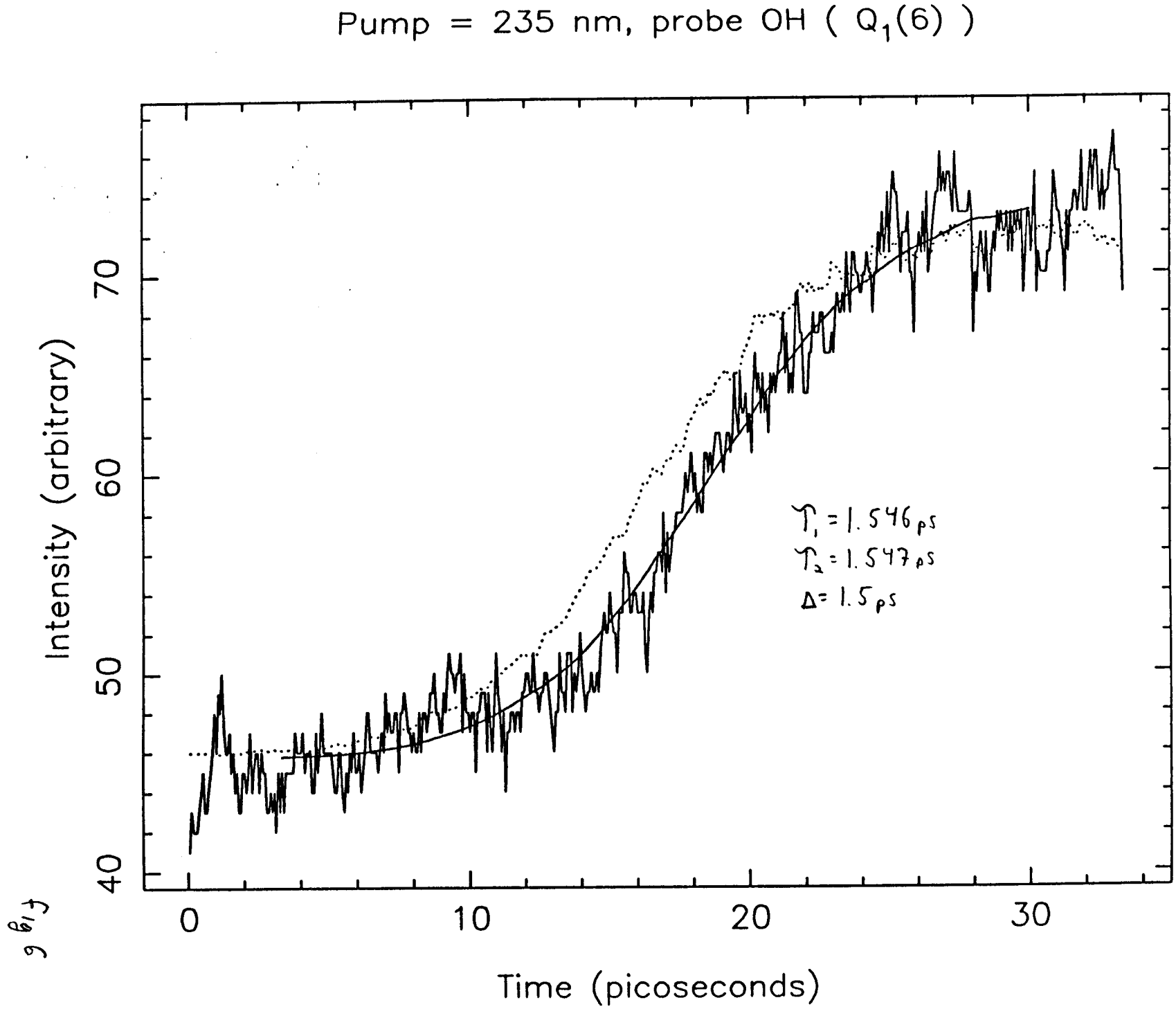
Pump = 235 nm, probe OH ($Q_1(6)$)
Intensity (arbitrary)
40
50
60
70
0
10
20
30
Time (picoseconds)
$\tau_1 = 1.546_{ps}$
$\tau_2 = 1.547_{ps}$
$\Delta = 1.5_{ps}$

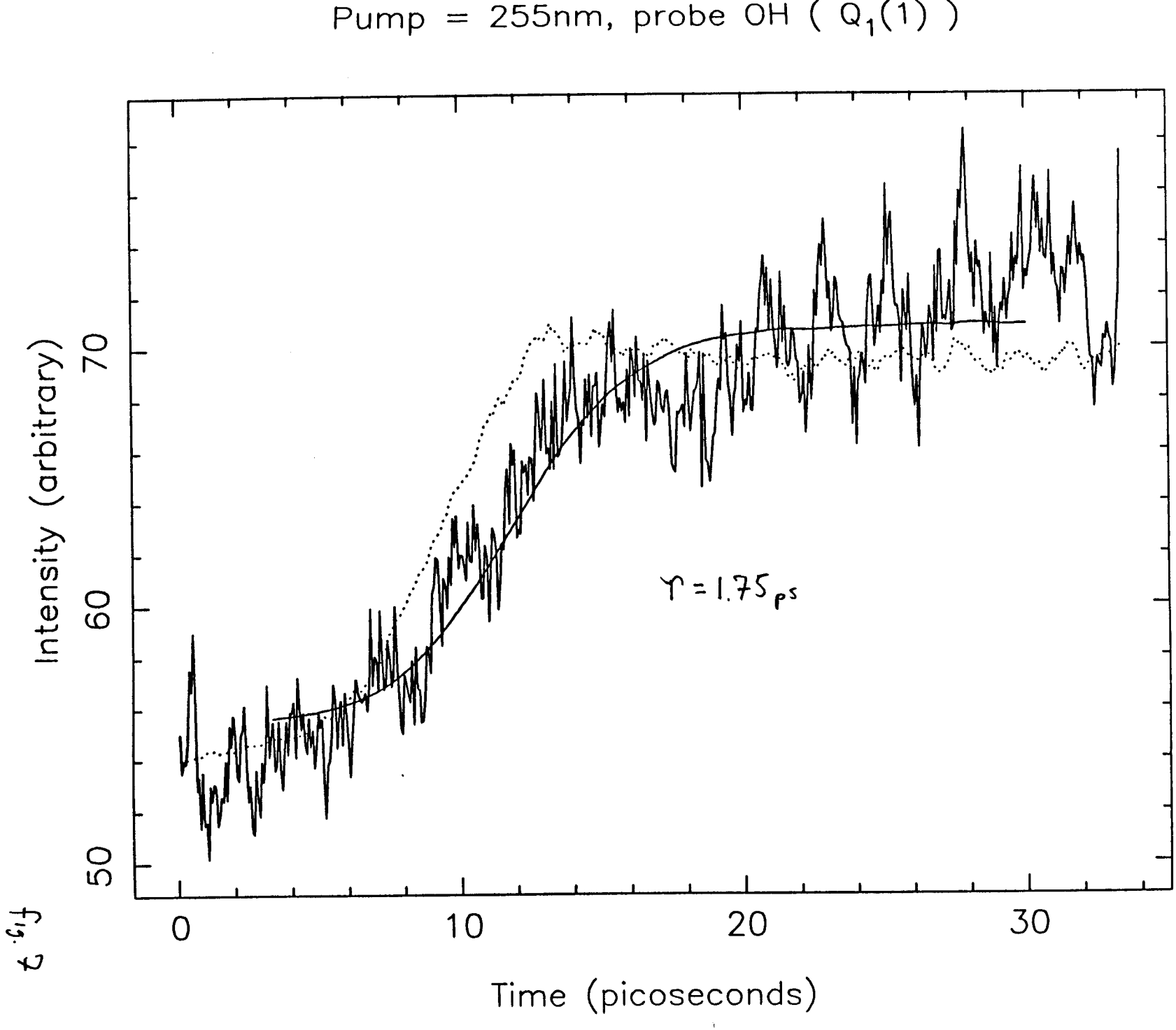
Pump = 255nm, probe OH ($Q_1(1)$)
Intensity (arbitrary)
50
60
70
0
10
20
30
Time (picoseconds)
$\tau = 1.75_{ps}$

fig 7

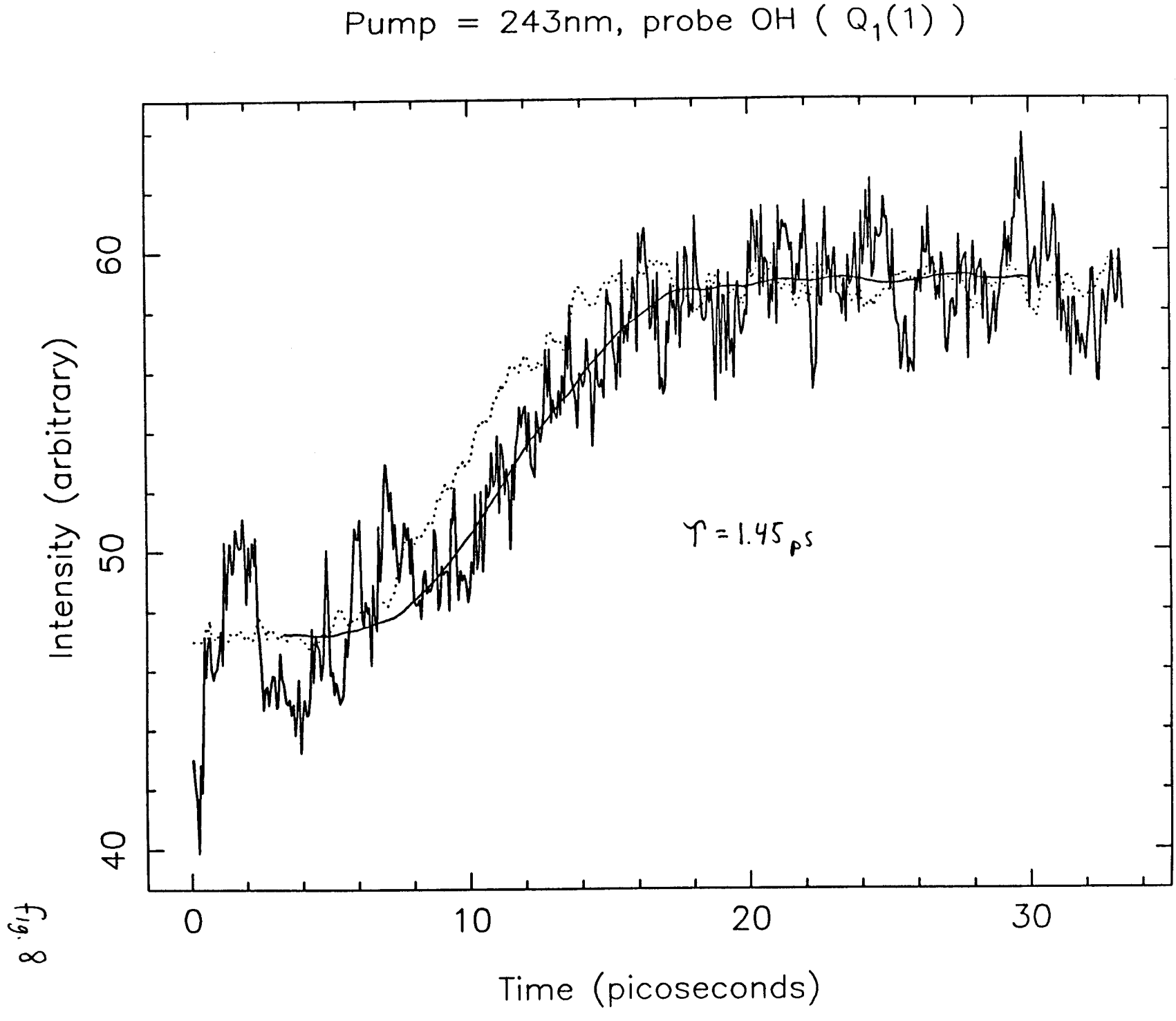
Pump = 243nm, probe OH ($Q_1(1)$)
Intensity (arbitrary)
40
50
60
0
10
20
30
Time (picoseconds)
$\tau = 1.45$ ps

Fig. 8

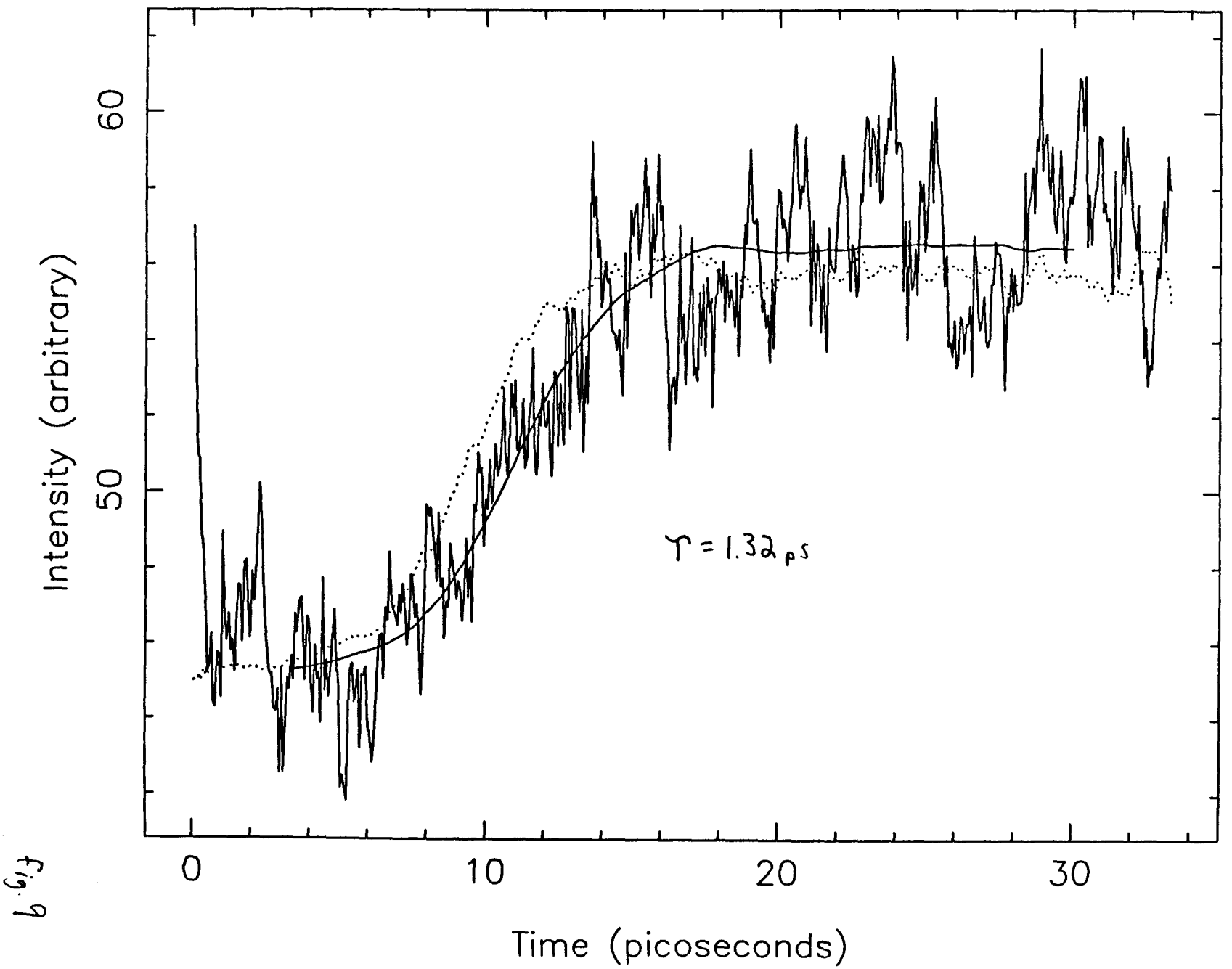
Pump = 241nm, probe OH ($Q_1(1)$)
Intensity (arbitrary)
50
60
0
10
20
30
Time (picoseconds)
$\tau = 1.32_{ps}$

fig. 9

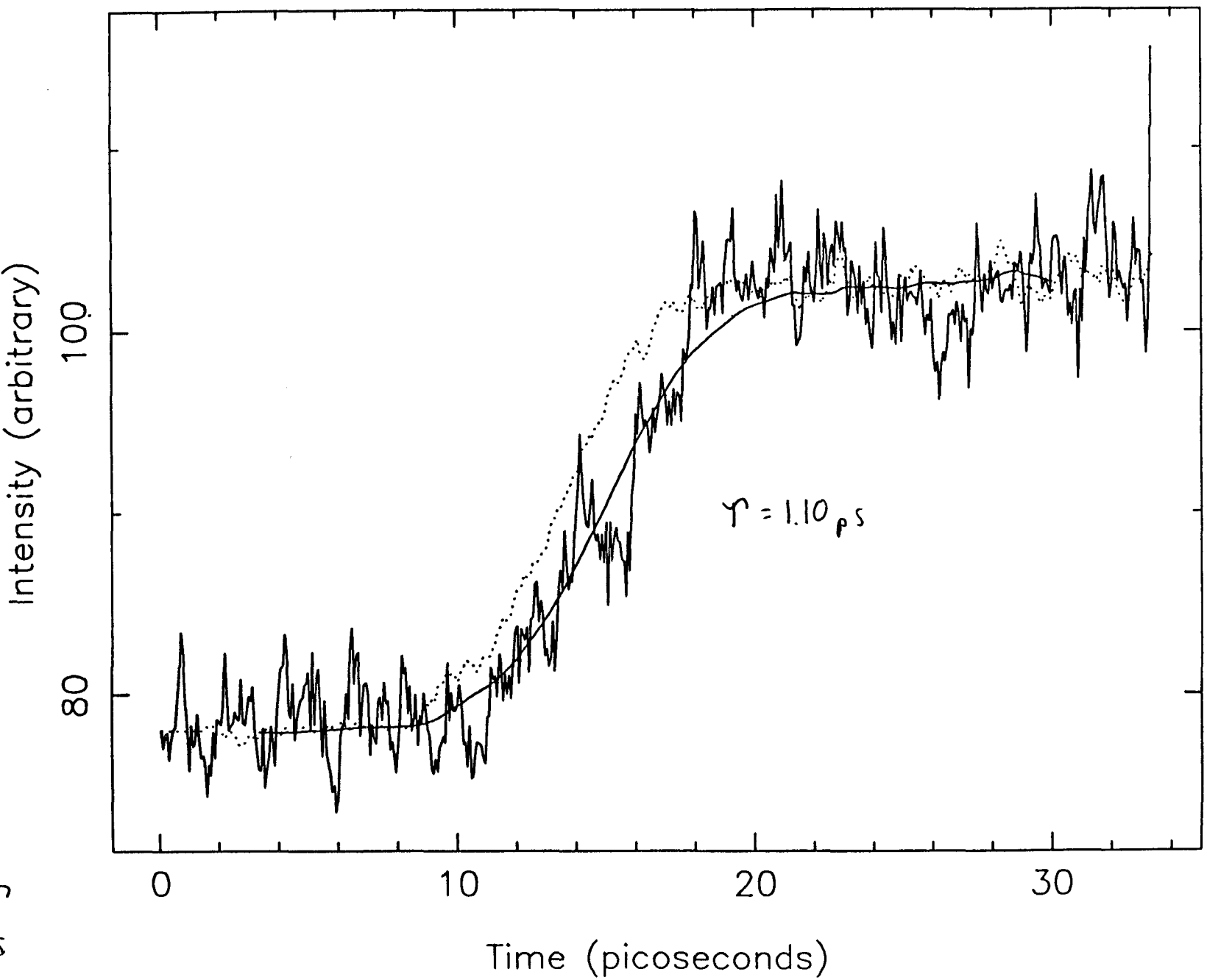
Pump = 239nm, probe OH ($Q_1(1)$)
Intensity (arbitrary)
100
80
0
10
20
30
Time (picoseconds)
$\tau = 1.10$ ps

fig. 10

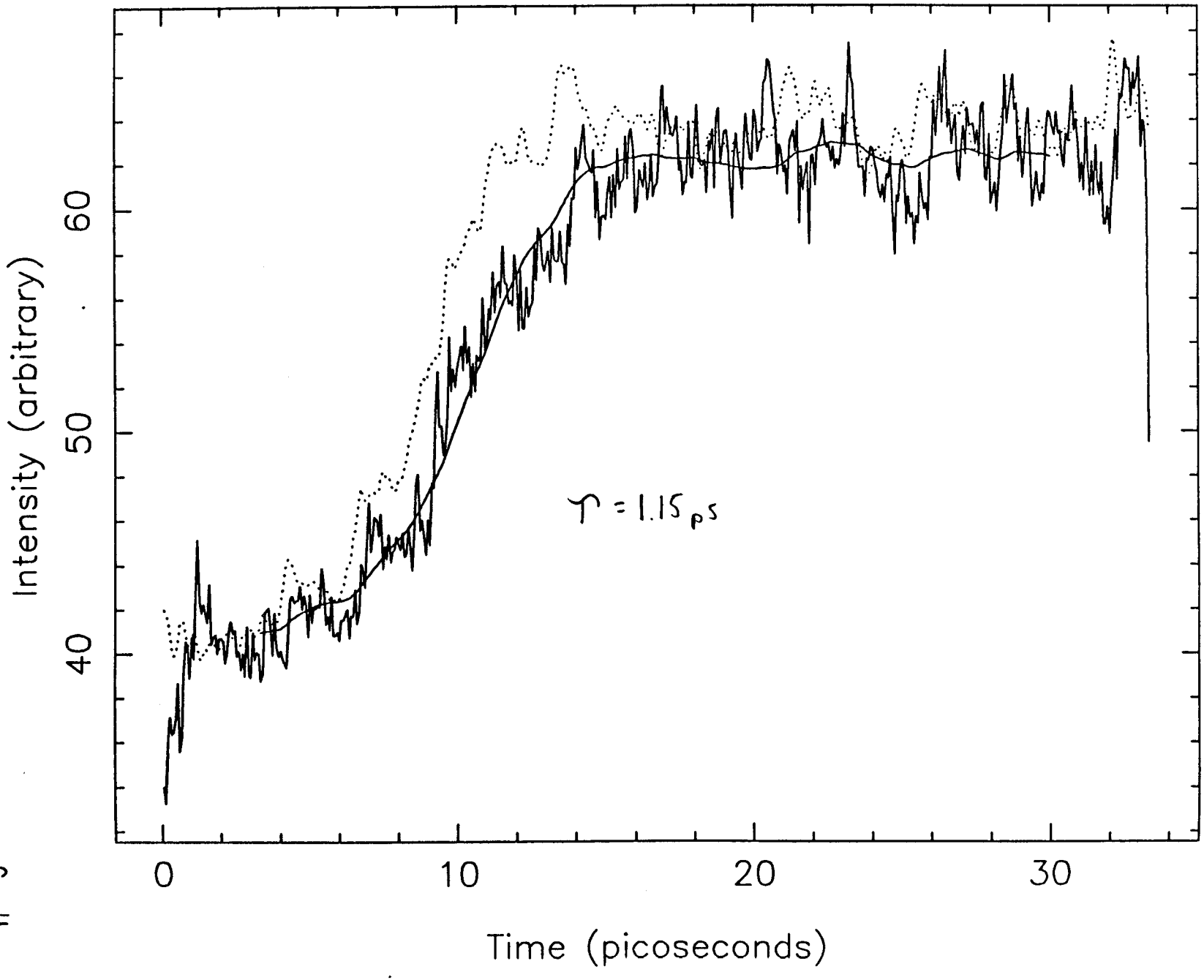
Pump = 237nm, probe OH ($Q_1(1)$)
Intensity (arbitrary)
40
50
60
0
10
20
30
Time (picoseconds)
$\tau = 1.15_{ps}$

Fig. 11

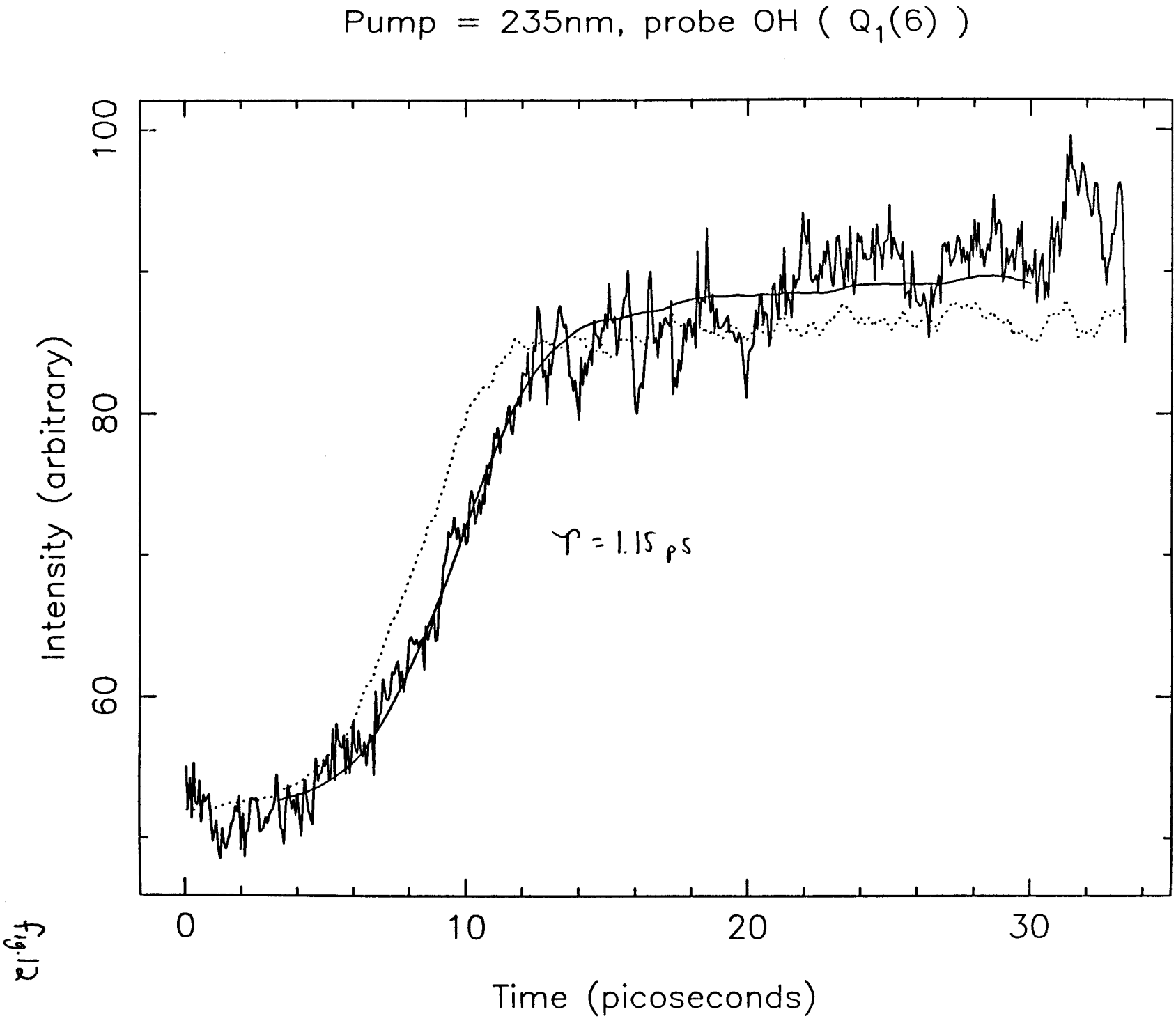
Pump = 235nm, probe OH ($Q_1(6)$)
Intensity (arbitrary)
100
80
60
0
10
20
30
Time (picoseconds)
τ = 1.15 ps

Fig. 12

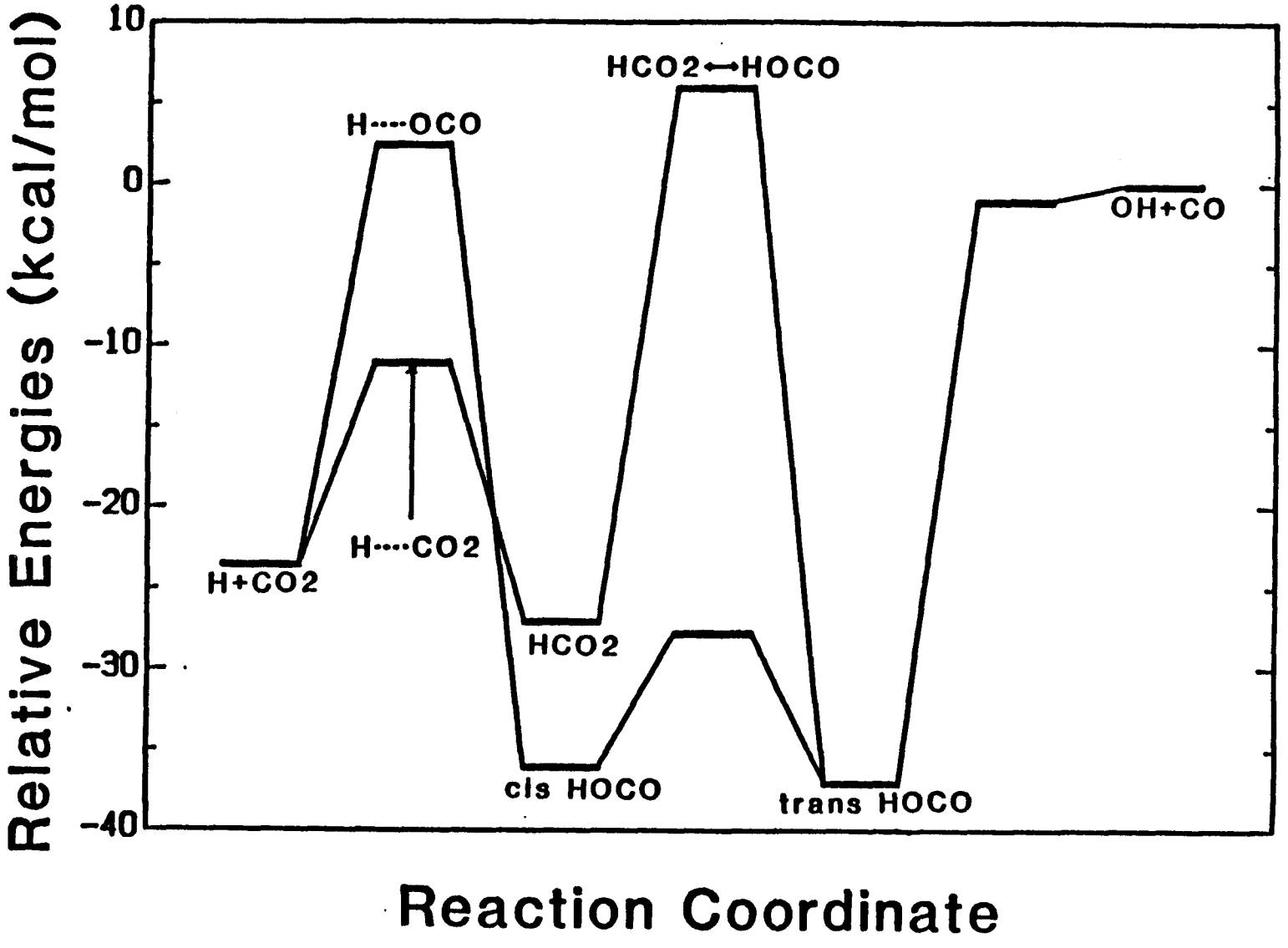
Relative Energies (kcal/mol)
10
0
-10
-20
-30
-40
H+CO2
H····OCO
H····CO2
HCO2
cis HOCO
HCO2←→HOCO
trans HOCO
OH+CO
Reaction Coordinate

Figure 13

Lifetime: HOCO => OH + CO

RRKM fit for I channel (fast H's)

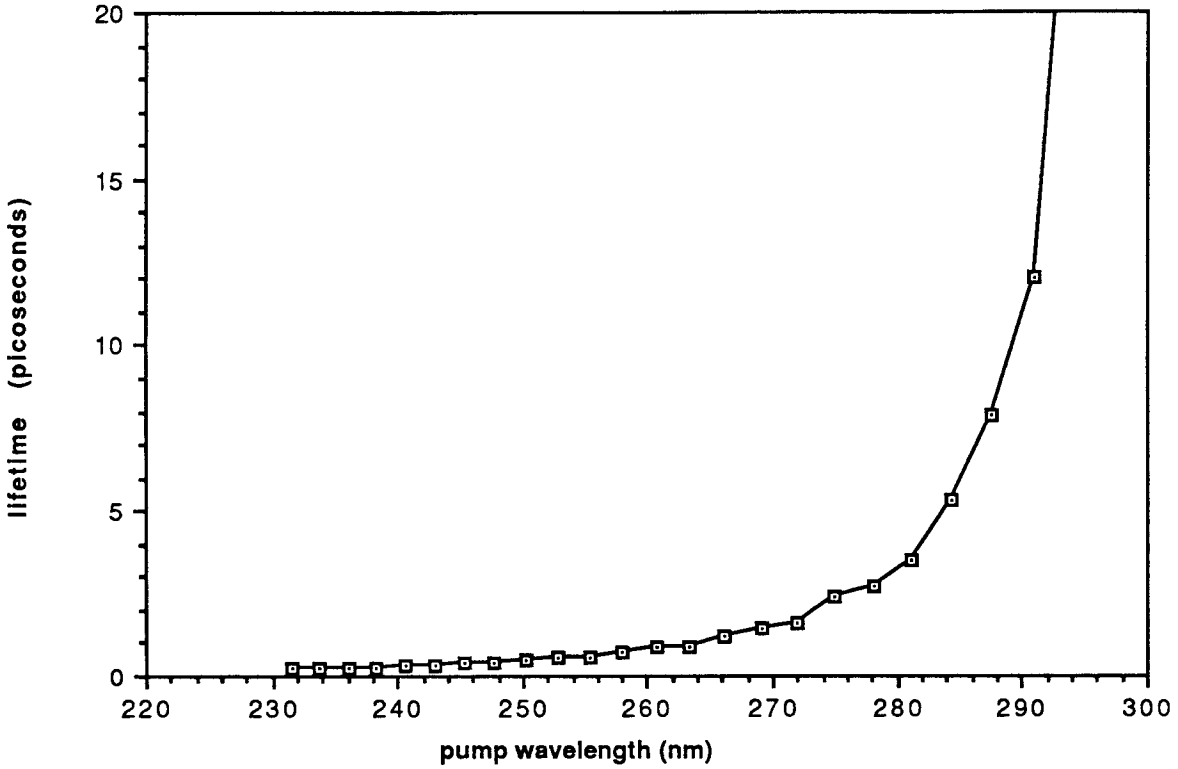

RRKM fit for I* channel (slow H's)

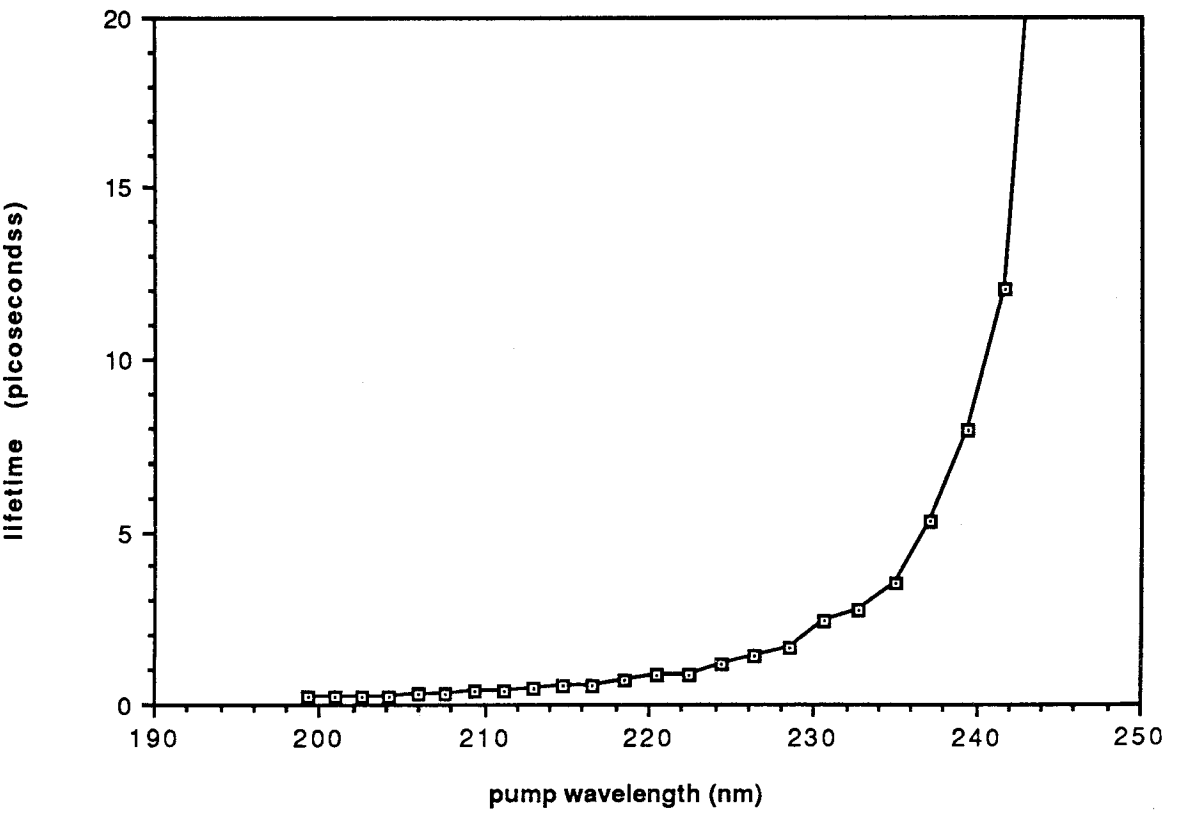

fig 14

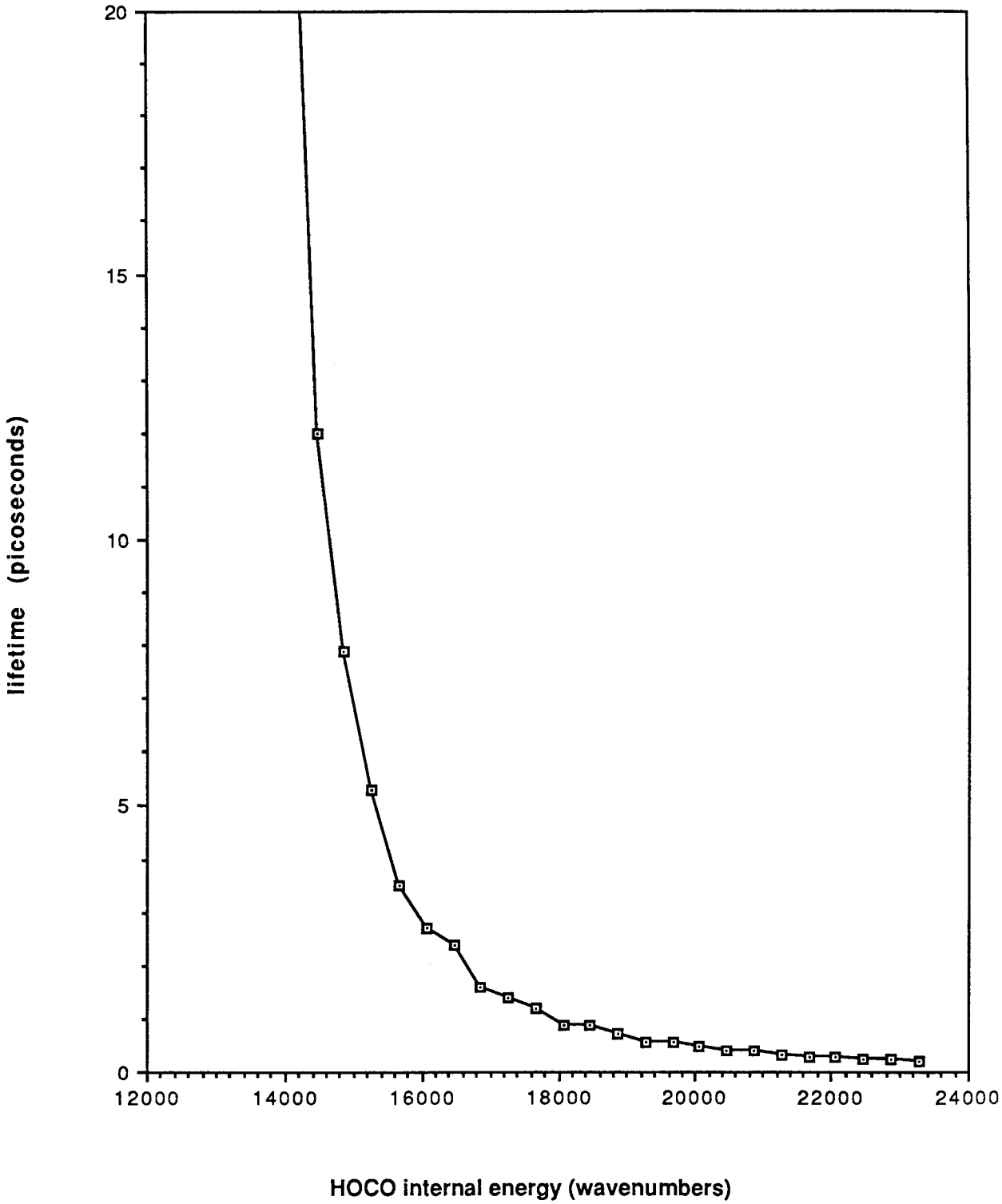
Lifetime: HOCO => OH + CO
RRKM fit vs Internal energy
lifetime (picoseconds)
20
15
10
5
0
12000
14000
16000
18000
20000
22000
24000
HOCO internal energy (wavenumbers)

Fig. 15a

Lifetimes from experiments and RRKM fits vs Internal energy

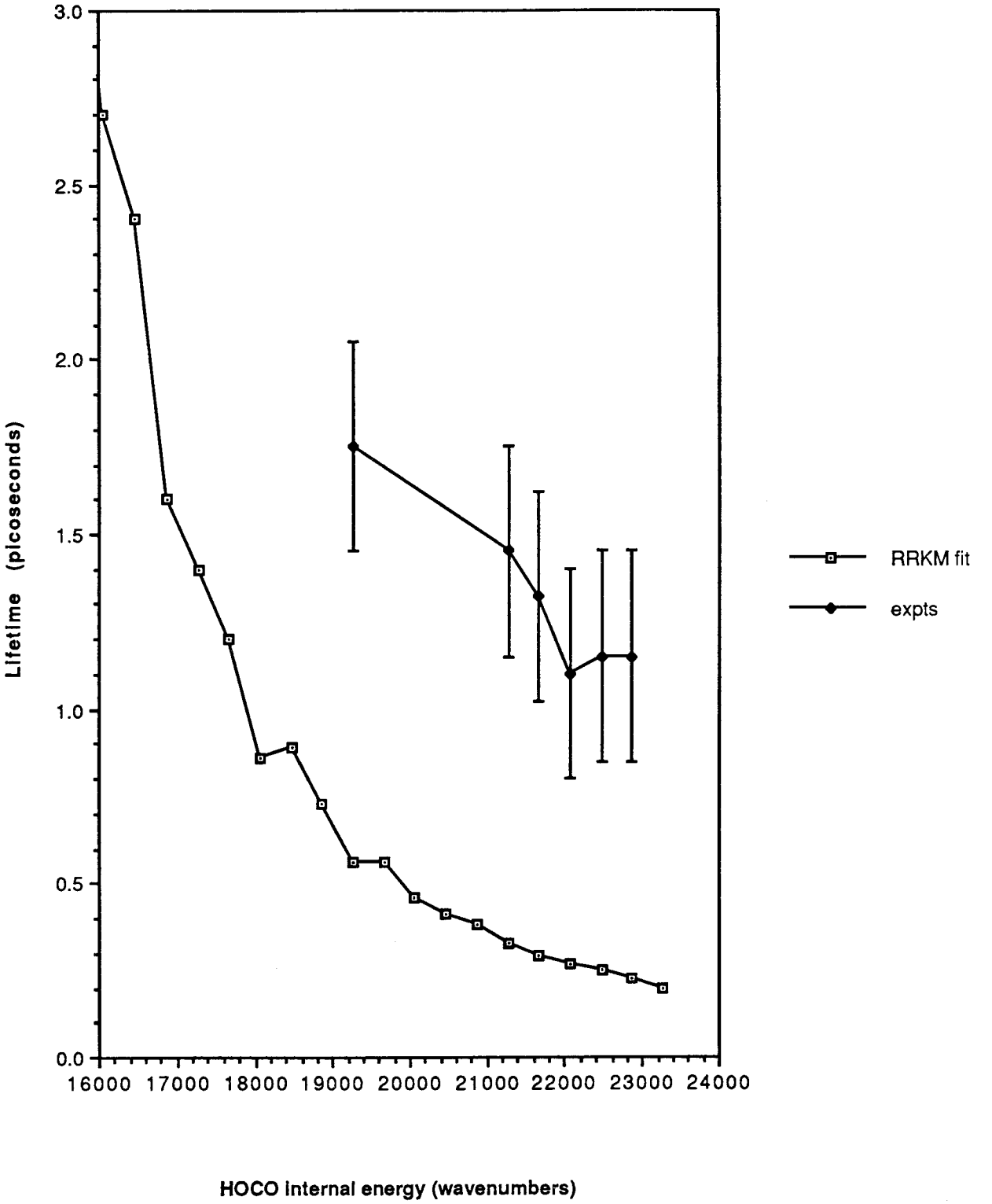

fig 15b

Proposition 1

Barriers to reaction of nucleophiles on trigonal carbons in the gas phase

Abstract

The nucleophilic attack on trigonal carbons in the gas phase differs from that in solution. Two reaction mechanisms have been proposed for the gas phase reaction, and evidence supporting both has been found. Although the double-well is preferred, problems with it remain, and solutions involving a single-well have been suggested. These mechanisms can be differentiated via their temperature-dependence, and an experiment to study this is proposed.

Nucleophilic attack upon the trigonal carbon of a carbonyl compound provides a useful synthetic route for a wide variety of molecules. As a result, the mechanism for nucleophilic displacement reactions (reaction 1) in solution is one of the most extensively studied. The most probable mechanism is the Bac2 reaction which proceeds with formation of a tetrahedral intermediate and its subsequent collapse into either products or reactants.[1-3]

$$X^- + RCOY \quad RCOX + Y^- \qquad (1)$$

In an attempt to study the intrinsic factors controlling the reactivities of carbonyl substrates without the complication of solvation, various attempts have been made to detect the formation of the tetrahedral intermediate in the gas phase.[2,4] In general, the effects of

solvation are difficult to predict, and the mechanism can undergo dramatic changes. Relative energy shifts -- due to unequal heats of solvation -- can change the reaction pathway and resulting products. The inhibition of the addition-elimination product appears to be a consistent trend. For instance, in solution, Sn2 attack of small nucleophiles upon esters is usually outcompeted by Bac2 attack. In the gas phase, this is reversed for a variety of esters (see Table 1). In fact, as demonstrated by reactions 2, the reaction may take alternate pathways even when carbonyl addition-elimination is energetically favorable.[3]

$$CH_3O^- + CH_3COF \Rightarrow CH_2COF^- + CH_3OH \qquad \Delta H = -18.4 \text{ kcal/mole}$$
$$\not\Rightarrow CH_3OHF + CH_2CO^- \qquad \Delta H = -20.3 \text{ kcal/mole}$$
$$\not\Rightarrow F^- + CH_3COOCH_3 \qquad \Delta H = -19.9 \text{ kcal/mole}$$

reactions 2

Clearly, the intrinsic (gas-phase) reactivity of the carbonyl group is very different from its reactivity in solution.

Two different mechanisms for reaction 1 have been advanced, each with a fundamentally different potential surface (see figure 1). The single-well potential, in analogy to the solvent phase, involves a tetrahedral intermediate which can collapse to either reactants or products.[5-7] In contrast, the double-well potential, as its name suggests, proposes two potential wells separated by a barrier of (usually) lower energy than reactants or products. The intermediates are now ion-dipole

Single-well Potential

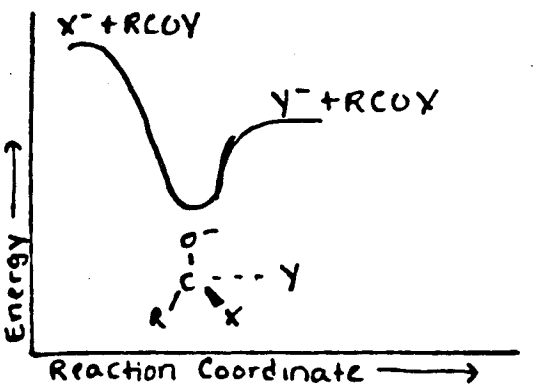

Double-well Potential

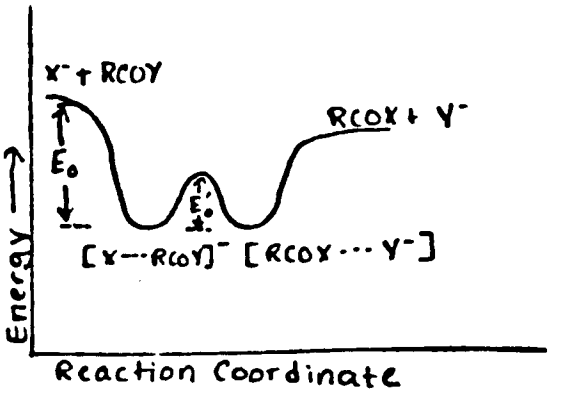

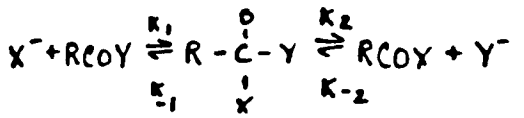

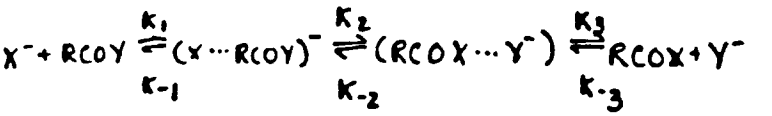

Fig. 1

clusters and the barrier is surmounted by a tetrahedral transition state.[3,8]

The evidence for a mechanism for reaction 1 can be divided into four categories. First, evidence for a tetrahedral structure in the reaction pathway. Second, *ab initio* studies of the energetics of the collision complex. Third, kinetic studies of the reaction efficiency (the fraction of collisions that result in reaction = $k/k_{collision}$). Fourth, thermodynamic analysis of the energies of proposed intermediates and transition states.

Asubiojo, Blair, and Brauman were among the first to announce evidence for a tetrahedral intermediate in the gas phase displacement reaction.[5] They studied the attack of halide ion on acyl halides. The intermediate in these reactions are able to transfer either ion to another acyl halide as shown in reactions 3.

$$F^- + CF_3COCl \Rightarrow CF_3COClF^- \; (+ CF_3COCl) \Rightarrow CF_3COCl_2^- + CF_3COF$$

$$CF_3CO^{35}Cl^{37}Cl^- + CF_3COCl \Rightarrow CF_3CO^{35}Cl^{35}Cl^- + \text{neutral}$$
$$\Rightarrow CF_3CO^{35}Cl^{37}Cl^- + \text{neutral}$$
$$\Rightarrow CF_3CO^{37}Cl^{37}Cl^- + \text{neutral}$$
reactions 3

The second piece of evidence is *ab initio* studies on the energetics of the reaction pathway.[7,9] They suggest a mechanism as follows[6]: As the nucleophile approaches the carbonyl group, the ion-dipole attraction decreases the potential energy of the system. At close range, the overlapping of molecular orbitals leads to an energy minimum at a tetrahedral configuration. The potential energy then increases as the intermediate breaks down and the new ion-molecule complex separates.

The third is kinetic investigations of the reaction. The obvious kinetic effect of the gas phase is the tremendous increase in rate. For instance, the reaction of hydroxide ion with methyl formate is about 10^{10} faster than in solution.[6] However, nucleophilic attack on carbonyl compounds in the gas phase, fast as it is, is not collision controlled; the reaction efficiencies are much less than one (see Table II). Reaction efficiencies this low, especially 0.05 for isotope exchange of chloride ion in acetyl chloride (reaction 1 of table II), suggest an internal barrier to the reaction. This can be easily shown via a kinetic analysis. The single-well potential leads to a rate constant and reaction efficiency

(assuming $k_{collision} = k_1$ since $E_a \sim 0$) as given in equations 1A and B[3,10]:

$$k = k_1 k_2/(k_{-1} + k_2) \quad (1A)$$

$$eff = k_2/(k_{-1} + k_2) \quad (1B)$$

In the case of isotope exchange, $k_{-1} = k_2$ and eff = 1/2. For exothermic reactions, $k_2 >> k_{-1}$ and eff ~ 1. This is clearly inconsistent with the data in Table II.

Asubiojo and Brauman, using RRKM analysis, correllated reaction efficiency to the height of the reaction barrier relative to reactant energies, for the double-well scheme. The calculation for the reaction of chloride ion with acetyl chloride is shown in Table III. The calculations predict an internal barrier of about 7kcal/mole below reactants. Since the binding energy of chlorine with acetyl chloride is estimated to be about 11kcal/mole,[3] this suggests an internal barrier to nucleophilic displacement about 4kcal/mole above the intermediates. Thus, the double-well mechanism is consistent with the kinetic data of Table II.

Clearly, the *ab initio* analysis, suggesting a single-well, is in disagreement with the kinetic data. Overall, the tendency is to accept the double-well hypothesis since the experimental work is more direct. Assuming a double-well mechanism with an internal barrier allows a calculation of the electron affinity of the tetrahedral radical using heats of formation derived by group additivity.[3] For the thermonuetral isotope

exchange reactions, the process gives an electron affinity very high for an alkoxy radical.[3] Since the mechanism does not require a tetrahedral transition state, it is possible that the barrier is surmounted by a different structure. However, by removing the tetrahedral transition state from the double-well mechanism, any connection is lost to the solution work. It also leaves in doubt the possible structure for the transition state. Since incorporation of the tetrahedral intermediate is very natural in the single-well mechanism, recent attempts have been made to reconcile this mechanism with the reaction inefficiency. In general, the question has been raised as to how a reaction efficiency can be lowered without the incorporation of a potential barrier.

In the gas phase, the excess energy of the collision complex is not carried off by collisions with other molecules. Nor is energy lost via radiation; the reagent pair thus have a constant total energy and angular momentum.[10] The stability of a compound relates to both its energy and how well it can partition its total energy among different states. Molecules with denser energy levels will be more stable. The need to partition energy is dramatically demonstrated in reaction 7 where the extra strain energy of methyloxetane drives the reaction to the enthropically favored products.[11]

NH_2^- + => $CH_2CHCH_2CH_2O^-$

NH_2^- + => $CH_2CHCH_2CH_2O^-$ => $CH_2CHCH_2^-$ + CH_2O

reactions 7

In the double-well model for the mechanism of reaction 1, the proposed tetrahedral transition state is "tighter" than the intermediate ion-molecule complexes.[3,10] The passage over the barrier is slow despite the fact that the complexes have the requisite energy. Moreover, the greater the temperature, the more energy the collision complex contains, and the more important the density of states in the reactants becomes. The collision complex more readily decomposes to reactants than it proceeds forward through the "tight" transition state; thus the efficiency decreases with increasing temperature.[10]

An entropic barrier may exist on the reaction pathway without the coexistence of an energy barrier. Kebarle describes the "locked-rotor" hypothesis as a mechanism which decreases the rate of reaction without erecting an internal barrier.[10] As the anion approaches the carbonyl compound, their external rotations may be restricted by steric effects. In a similar fashion to that above, this causes a decrease in reaction efficiency. The reaction would also exhibit *negative temperature* dependence. The locked-rotor hypothesis could possibly explain the kinetic data of Table II without necessitating a double-well potential.

Recently, a number of theoretical studies have been undertaken of the ability of rotational barriers to reduce reaction efficiencies. Clary, for instance, has shown the efficacy of the centrifugal barrier to hinder reaction both in neutral[12] and ion-molecule[13] reactions. This centrifugal

barrier does require an increase in the potential energy, in contrast to the locked-rotor hypothesis which is entropic in nature. However, both reduce the reaction efficiency without invoking a double-well potential and both are marked by negative temperature dependence.

In the case of a double-well potential, in which the internal barrier is above the level of the reactants, the reaction would show positive temperature dependence, since additional energy would be needed to surmount the barrier.[10] Thus, by varying the "R" in reaction 8, from electron withdrawing to electron donating, the internal barrier (if one exists) will increase in energy.

$$X^- + RCOY \Longleftrightarrow [X\cdots RCOY]^- \Longleftrightarrow [RCOXY]^{\dagger -} \Longleftrightarrow [RCOX\cdots Y]^- \Longleftrightarrow RCOX + Y^- \quad (8)$$

When the barrier becomes higher than the energy level of the reactants, the temperature dependence should switch. This switch is characteristic of an internal energy barrier; its occurrence would strongly substantiate the double-well mechanism for the reaction pathway of nucleophilic displacement on carbonyl carbons.

REFERENCES

(1) M. Comisarow. *Can. J. Chem.* **1977**, 55,171.

(2) O. I. Asubioja; L. K. Blair; and J. I. Brauman. *J. Am. Chem. Soc.* **1975**, 97, 6685.

(3) O. I. Asubioja and J. I. Brauman. *J. Am. Chem. Soc.* **1979**, 101, 3715.

(4) J. H. Bowie and B. D. Williams. *Aust. J. Chem.* **1974**, 27, 1923.

(5) S. M. Jose and J. M. Riveros. *Nouv. J. Chim.* **1977**, 1, 113.

(6) K. Takashima and J. M. Riveros. *J. Am. Chem. Soc.* **1978**, 100, 6128.

(7) G. Alagona; E. Scrocco; and J. Tomasi. *J. Am. Chem. Soc.* **1975**, 97, 6976.

(8) J. E. Bartmess; R. L. Hays; and G. Caldwell. *J. Am. Chem. Soc.* **1981**, 103, 1338.

(9) I. H. Williams; G. M. Maggiora; and R. L. Schowen. *J. Am. Chem. Soc.* **1980**, 102, 7831.

(10) T. F. Magnera and P. Kebarle in "Ionic Processes in the Gas Phase". M. A. Almoster Ferreira, ed.; (NATO ASI Series C, Volume 118); Reidel: Boston **1984**.

(11) C. H. Depuy and V. M. Bierbaum. *Acc. Chem. Res.* **1981**, 14, 146.

(12) D. C. Clary *Mol. Phys.* **1984**, 53, 3.

(13) D. C. Clary *Mol. Phys.* **1985**, 54, 605.

TABLE I

Rate constants for carboxylate and alkoxide formation[5]
(Rate constants in units of 10^{-10} cm^3 mol^{-1} s^{-1})

$F^- + RCOOR' \Rightarrow RCOO^- + neutrals$ ($k_{carboxylate}$)

$F^- + RCOOR' \Rightarrow RCOF + R'O^-$ ($k_{alkoxide}$)

ester	$k_{carboxylate}$	$k_{alkoxide}$	$k_{carb.}/k_{alkox}$
$CH_3COOC_2H_5$	1.6	0.4	3.6
$CH_3COOCH_2CH_2CH_3$	1.6	0.9	1.8
$CH_3COOCH(CH_3)_2$	2.5	0.5	4.9
CH_3COOCH_3	0.6	0.3	1.7
$C_2H_5COOC_2H_5$	4.7	0.2	25

TABLE II

Reaction Efficiencies for Nucleophilic Attacks (ref. 3)

Reaction	Efficiency
(1) $^{37}Cl^- + CH_3CO^{35}Cl \Rightarrow {}^{35}Cl^- + CH_3CO^{37}Cl$	0.05
(2) $^{37}Cl^- + CH_3CH_2CO^{35}Cl \Rightarrow {}^{35}Cl^- + CH_3CCH_2O^{37}Cl$	0.032
(3) $^{37}Cl^- + (CH_3)_2CHCO^{35}Cl \Rightarrow {}^{35}Cl^- + (CH_3)_2CHCO^{37}Cl$	0.027
(4) $^{37}Cl^- + (CH_3)_3CCO^{35}Cl \Rightarrow {}^{35}Cl^- + (CH_3)_3CCO^{37}Cl$	0.028
(5) $F^- + (CH_3)_3CCOCl \Rightarrow Cl^- + (CH_3)_3CClF$	0.15
(6) $F^- + CF_3COCl \Rightarrow Cl^- + CF_3COF$	0.23

TABLE III

RRKM calculation of barrier height (E-E') in kcal/mol
for the reaction $Cl^- + CH_3COCl \Rightarrow Cl^- + CH_3COCl$ (ref. 3)

E-E'	eff.	E-E'	eff.
10.0	0.30	7.0	0.06
9.0	0.21	6.0	0.03
8.0	0.13	5.0	0.01

Proposition 2

Measurement of the rate of formation of SD from the photodissociation of the complex ID···OCS

Abstract

Recently, Wittig and coworkers have studied the reaction of D + OCS to give OD and CS or SD and CO in the gas phase.[3] In a molecular beam, the cluster XD···OCS is formed with a linear geometry and in the configuration shown. Unfortunately, Wittig was not able to resolve the SD formed by dissociating the BrD molecule in this cluster. This is a very interesting reaction because of the need for the deuterium to migrate to the sulfur atom. We propose an experiment to resolve this rate by dissociating the complex ID···OCS.

As has been previously described above, the photodissociation of certain van der Waals clusters can be used to study energy redistribution in bimolecular reactions with constrained attack parameters. For instance, via fragmentation of the hydrogen-halogen bond in the complex XH···OCO, hydroxyl radical was formed from solely end-on attack in the reaction H + CO_2 => OH + CO.[1,2] The intermediate in in this reaction, HOCO, was found to have a surprisingly long lifetime[2] and yield products with a rotational distribution colder than in the bulk reaction.[1] In this report, we propose to study the reaction D + OCS => DS + CO in a precursor

limited geometry.

The reaction of deuterium atoms with carbonyl sulfide, both in the gas phase and under molecular beam conditions, has recently been studied by Wittig and coworkers.[3] The reaction was observed to have two product channels:[3]

$$D + OCS \Rightarrow DO(X^2\Pi) + CS(X^2\Sigma) \qquad \Delta H = 55\text{kcal/mole} \qquad (1)$$
$$\Rightarrow DS(X^2\Pi) + CO(X^2\Sigma) \qquad \Delta H = -10\text{kcal/mole} \qquad (2)$$

In the gas phase study, DBr and OCS were introduced into a flowing cell at 10-60mtorr pressure. A pulse of 193nm light dissociated the deuterium bromide, producing a deuterium atom with 60kcal/mole of energy. This is sufficient energy to follow either product channel, and indeed, Wittig observes both OD and SD products. The OD fragments were probed via LIF following 308nm electronic excitation and the SD via LIF following 323nm excitation (in both cases $^2\Pi \Rightarrow {}^2\Sigma$ transitions). The use of deuterium was necessitated by the fast predissociation of HS which restricts LIF[4,5] (since the fragment will dissociate before it radiates).

Since they were able to resolve individual rotational lines, both the relative populations of different product channels (1 and 2 above) and of different rotational levels could be calculated. About five times as much SD as OD is formed by a 60kcal/mole deuterium, and both products seemed to have statistical rotational distributions.[3] This suggests that the reaction goes through some sort of intermediate (probably DOCS or OCSD)

in which energy has an opportunity to redistribute.[3] In both cases, the average rotational energy is small. Only about 1kcal/mole, of an available 70, ends up in SD rotation.[3] Wittig suggests that after formation of the SD bond, the C-S coordinate becomes steeply repulsive. Since the center of mass of the fragment lies very near the sulfur, very little torque is applied to the SD.

In order to study the reaction in the molecular beam, they seeded the beam with both deuterium bromide and carbonyl sulfide. This produced the complex BrD···OCS which was then photodissociated with 193nm light. This cluster has not been studied, but several groups have studied FH···OCS.[6,7] They found that the complex had a linear geometry. Moreover, FH···SCO was not detected in either study. Thus, Wittig makes the reasonable assumption that the bromide cluster would also be linear and complexed to the oxygen end. With this assumption, they then proceeded to study the PLG reaction of D + OCS with the angle of attack limited to end-on on the oxygen.

Wittig had hoped to observe the rotational distributions of SD formed in this manner. Unfortunately, this proved impossible. DBr and OCS react on surfaces to yield D_2S.[3] The deuterium sulfide also absorbs 193nm light, after which it dissociates to form DS and D.[8,9] The absorption cross-section for hydrogen sulfide is seven times larger than hydrogen

bromide at 193nm;[10] even a small amount of deuterium sulfide would produce an amount of SD commensurate with that from the desired reaction. This process could be avoided in the gas-phase studies by flowing the two gases through separate inlets. However, in the molecular beam, the two gases must be expanded together, and so some deuterium sulfide is formed in the nozzle plenum.[3] This prevents the measurement of the SD rotational distribution formed by end-on attack on the oxygen.

We believe that with picosecond pump-probe techniques, we will be able to study the PLG reaction of D + OCS. In this case, we propose to form the ID···OCS cluster. In analogy to Wittig's work, we will assume that this is linear and forms exclusively in the relative orientation shown. In our case, we will photofragment the deuterium iodide with a picosecond pulse of 250nm light. Deuterium iodide is commercially available, and we can generate light from 266 to 220 nm via continuum generation, amplification with coumarin dye,[11] and subsequent second harmonic generation. At 250nm, the cross-section for absorption in HI is ten times that of H_2S,[10] a factor of seventy better than in Wittig's study. Moreover, if need be, we can vary the wavelength out to 266nm. At this wavelength, HI absorbs fifty times more strongly than H_2S.[10] We believe that this will sufficiently minimize the formation of DS from D_2S as to allow the resolution of DS from the PLG reaction.

We believe that this reaction is an extremely interesting one to study. With a 250nm excitation pulse, the deuterium atom will carry 37kcal/mole. This is not enough to allow formation of OD; the only product channel is SD formation. However, the PLG conditions do not allow deuterium capture by the sulfur,[3] thus the atom must be captured by the oxygen. Product formation will occur via deuterium migration. We would then be able to measure the rate at which an intermediate is able to transfer a light atom.

If, in fact, these measurements show a long lifetime for the intermediate, say around 5ps, then we will be able to extend the study to higher energies. In this case, SD formed via the PLG reaction can be distinguished temporally from that formed from deuterium sulfide dissociation. The electronic predissociation of H_2S has been suggested to occur in about 18fs at a dissociation wavelength of 222nm.[12] If we use 220nm light for our pump, then the risetime of SD product should show two lifetimes, one of which (from D_2S) will be faster than our resolution. If we can resolve the second lifetime, then this one will be the lifetime of the intermediate formed by reaction of deuterium with carbonyl sulfide under PLG conditions. The advantage of extending this study down to 220nm is that this will produce a deuterium with around 60kcal/mole. At this energy, it is likely that we will also be able to observe formation of

OD. This will allow us compare the tendency for the initially formed intermediate, DOCS, to proceed via the higher energy, more direct product channel, OD and CS formation, rather than undergo an isomerisation in order to form the more stable products.

REFERENCES

(1) S. Buelow; G. Radhakrishnan; J. Catanzarite; and C. Wittig *J. Chem. Phys.* **1985**, 83, 444.

(2) N. F. Scherer; L. R. Khundkar; R. B. Bernstein; and A. H. Zewail *J. Chem. Phys.* **1987**, 87, 1451.

(3) D. Hausler; J. Rice; and C. Wittig *J. Phys. Chem.* **1987**, 91, 5413.

(4) J. J. Tiee; M. J. Ferris; and F. B. Wampler *J. Chem. Phys.* **1983**, 79, 130.

(5) R. R. Friedl; W. H. Brune; and J. G. Anderson *J. Chem. Phys.* **1983**, 79, 4227.

(6) F. A. Baiocchi; T. A. Dixon; C. H. Joyner; and W. Klemperer *J. Chem. Phys.* **1981**, 74, 6544.

(7) J. A. Shea; W. G. Read; and E. J. Campbell *J. Chem. Phys.* **1983**, 79, 614.

(8) C. F.Goodeve and N. O. Stein *Trans. Faraday Soc.* **1931**, 27, 393.

(9) K. Watanabe and A. S. Jura *J. Chem. Phys.* **1964**, 41, 1650.

(10) Calculated using J. Huebert and R. M. Martin *J. Phys. Chem.* **1968**, 72, 3046, and references 8 and 9.

(11) D. M. Guthals and J. W. Nibler *Opts. Commun.* **1979**, 29, 322.

(12) G. N. A. Van Vleen; K. A. Mohamed; T. Baller; and A. E. Devries *Chem. Phys.* **1983**, 74, 261.

Appendix I

Off-Resonant Absorption From OH on the Peroxide Dissociative Surface

Introduction

In a series of papers dating back to 1981, Polanyi and coworkers describe a technique to take advantage of so-called wing-emission from perturbed species.[1] In particular, they have observed emission from excited sodium atoms produced in the photodissociation of NaI.[1b] Via a monochrometer, Polanyi selectively observes the light emitted to the red of the free sodium D line. He reasons that this light must come from sodium atoms whose states are still perturbed by their iodine partners; in other words, from sodium iodide in the process of falling apart. Since this technique allows the investigator to distinguish light emitted on the dissociative surface, Polanyi hopes that it will help to elucidate the mechanisms of photodissociation reactions which are typically too fast to observe in a more conventional manner.[1]

Recently, in the Zewail group, we have conducted pump-probe experiments similar in spirit to Polanyi's.[2] Here, a pump laser pulse of a few picoseconds or shorter duration initiates the direct dissociation of a molecule and a second pulse, tuned off the free product absorption, promotes the dissociating species to a higher surface yielding excited

fragments. The emission from the excited fragments is then imaged onto a photomultiplier. The additional flexibility provided by the second laser pulse enables us to investigate fragmentation on surfaces which produce ground-state products. We have generalized the technique in order to apply it to a variety of different systems: to date, we have observed off-resonance absorption in a femtosecond photofragmentation of ICN,[2a,c] a picosecond photoionization of CH_3I in a supersonic expansion,[2b] and -- the subject of this report -- in a picosecond study of the rotationally resolved OH products in the photodissociation of H_2O_2.

Temporal Resolution in Off-Resonant Absorption

In the femtosecond study,[2a,c] the correlation between the frequency of the absorbed light and the distance along the dissociative surface (i.e., the time since the fragmentation began) could be confirmed by actual resolution of the rise and fall times of the absorption. In this case, absorption to the red of the nascent cyanyl peak was seen to rise and fall within a few hundred femtoseconds. The decline in absorption to the red was complemented by the rise in on-resonant absorption. This result is rationalized by the intuitive concept of the transition state, here the species I···CN, which has an electronic absorption to the red of the bare CN radical. The amount which the absorption red shifts decreases as the separation between fragments increases, asymptotically becoming

indistinguishable from bare CN.

As with ICN,[3] the direct dissociation of hydrogen peroxide is essentially complete -- which term, in the context of this experiment, means that the fragment absorption spectrum is indistinguishable from that of the unperturbed molecule -- in a few hundred femtoseconds,[4] much faster than the resolution of the picosecond instrument. The convolution of the rise-time with the laser pulse is indistinguishable with the convolution of a delta function with the laser pulse; this means that we are not able to temporally distinguish the absorption of the so-called transition state (i.e., any species of the form HO···OH on the dissociative surface) from the separated fragment; both on- and off- resonance absorption show the same rise-time. This is not to suggest that both wing and resonant absorption have the same temporal behavior. As can be seen in figures 1, off-resonant absorption shows a drop after the initial rise. Once we are off-resonance, the species absorbing during dissociation compose a significant fraction of the molecules we are probing. This species will exist for a fraction of a picosecond after the absorption of the pump photon. The amount emission from excited hydroxyl will depend upon the transition moment for the absorption, weighted by the length of time this species lives, and the overlap of the pump and probe pulses. The off-resonant absorption will have the temporal profile of a cross-correlation between the two laser pulses, and

the relative magnitudes at different wave-lengths will depend upon the probability of absorption of the particular photon. We have paid a price for our lack of temporal resolution; we are unable to temporally distinguish the transition state. Instead, since we have approximately 5cm^{-1} pulses (as opposed to the 200cm^{-1} pulses in the femtosecond regime), we are able to take a spectral profile of the absorption due to a dissociating species. We will be able to take advantage of our increased spectral resolution to probe further our notions of just what the probability of absorption of a particular photon will be.

Experimental Details

The experimental apparatus has been described elsewhere.[5] The fragmentation of hydrogen peroxide is initiated by an approximately 5ps laser pulse at 266nm. A second laser pulse, delayed in time, excites the resulting fragments via the $^2\Pi \Rightarrow {}^2\Sigma$ electronic transition. The resulting spontaneous emission is collected, and the total emitted light is proportional to the population probed. By varying the delay, the change in fragment population with time is measured. The rotational constant B of hydroxyl is ~18cm^{-1},[6] so we are able to resolve certain rotational lines.

At room temperature, the internal energy content of the peroxide molecules is ~400cm^{-1}. Since a 266nm photon contains 37,000cm^{-1} and two $^2\Pi$ hydroxyls lie 17,300cm^{-1} above the ground-state peroxide well,[7] 20,700cm^{-1} is available for fragmentation. This energy is not sufficient

for electronic excitation of OH, and indeed no emission from the $^2\Sigma$ state is observed.[4] From measurements of the doppler shift in absorption by the recoiling photofragments, the translational energy of the hydroxyl radicals was found to be (20,000 ± 1,000)cm^{-1}.[4b] The fragments are all moving at a velocity within 5% of 37Å/ps. Overall, 90% of the energy goes into translation, 10% into rotation, and less than 0.2% into vibration.[4b] In many ways, this distribution makes the dissociation a particularly amenable one for study. The narrow spread in fragment velocity allowed a particularly thorough analysis of the product vector correlations.[4b,8,9] Moreover, a large B not only spreads out the different rotational transitions but also produces a narrow rotational distribution. This means that a sizable fraction of the population is in each rotational level, which facilitates experimental resolution. We believe that this is a particularly good system with which to begin an analysis of the spectral features of off-resonant absorption.

Dynamics of the Photodissociation

The choice of 266nm for our dissociation wavelength was not arbitrary. Much is known about the orientation of products from photodissociation at this wavelength due to studies of the product vector correlations,[4b] following a scheme detailed by R. N. Dixon.[9b] As mentioned above, this study was greatly facilited by the narrow translational energy distribution. Also helpful was the promptness of the

dissociation.[4] Since the photoexcited parent is very short-lived and the recoil velocity is much larger than the rotational velocity of the peroxide, parent rotation should not greatly affect the distribution of OH fragments, and the observed translational and rotational anisotropy will therefore reflect the dynamics of the dissociation.[4,10]

Particularly helpful for our study was the measurement of the bipolar moment $\beta_0^0(2\ 2)$,[4b] which reflects the correlation between the fragment angular momentum and recoil velocity. In this case, $\beta_0^0(2\ 2)$ was found to be very close to its limiting value, particularly as J_{OH} increased.[4b] This means that the fragments show a strong tendency to align their angular momenta parallel to their recoil velocity. If we assume a purely axial recoil, then the planes of rotation of the two fragments are essentially parallel to each other and perpendicular to the intermolecular axis.

This can be easily rationalized.[11] Since the center-of-mass of the OH fragment lies very close to the oxygen atom, the recoil along the O-O bond of the excited peroxide will apply very little torque. Though some fragment angular momentum will be imparted via vibrational motion, the vibrational modes of peroxide are not extensively populated at room temperature. Hence, the primary source of fragment rotation is suggested[4,8,12] to be a strong torsional dependence of the repulsive surface, which, naturally, would produce fragments whose angular

momenta were aligned with their velocities.

Fragment Absorption on the Dissociative Surface: Core Repulsion and Long Range Interactions

After excitation to the repulsive surface, the two fragments will recoil away from each other, quickly converting most of the potential energy into kinetic. Initially, most of the energy deposited in the molecule is in the form of potential, the interaction of the fragments dominated by core repulsions due to the substantial overlap of the charge clouds of the two soon-to-be-hydroxyl fragments. The two relevant dissociative surfaces, that leading to two $^2\Pi$ hydroxyl fragments and that leading to one $^2\Pi$ and one $^2\Sigma$ fragment, should approach each other, since the wave functions for the two different electronic states of OH differ more in their outer than their inner regions. Thus, absorption at small O-O internuclear separation should show a red shift relative to the nascent electronic transition. [N.B. This is essentially the same logic that is used to rationalize the red wing-emission in NaI dissociation[1b] and red-shifted absorption in ICN.[2a,c] While we expect a similar effect in most systems, it is certainly not required, and some systems may in fact show a blue shift.] The two surfaces may converge substantially as the O-O distance decreases, and we might expect to see absorption far to the red, perhaps many angstroms. This tendency, however, will be counterbalanced by the low probability of probing the fragments in a particular wavelength

interval. In this region, the surfaces are steeply repulsive,[12] and the difference between them is changing rapidly. Thus, the exponentially repulsive part of the potential should be characterized by a broad, red-shifted absorption.

As the internuclear separation increases, the fragment velocities approach their asymptotic values and the potential levels off. In this region, the energy levels for the fragments are almost, but not quite, those of the unperturbed species. The interaction between the fragments in this region of the excited state surface is dominated by long-range forces,[13,14] such as dipole-dipole and dipole-quadrupole, and these forces may still be strong enough to perturb the energy levels to a measurable degree.

In order to more closely analyze these two regimes, we need to model the two dissociative surfaces. Typically, we can model the repulsive region as an exponential,[2c,12] $V \sim \exp(-R/L)$, where R is the fragment separation and L, a constant, is a characteristic of each surface. The lower surface, leading to two $^2\Pi$ hydroxyl radicals, has been well modelled by Bersohn and Shapiro.[12] The form for the lower potential that Bersohn and Shapiro fit, ignoring the torsional angle dependence, is:[12]

$$V = 704\text{eV} \exp(-R/0.266\text{A})$$

The interaction energy due to this potential is only 1.7cm^{-1} at 4Å, the

distance at which the authors suggest long-range forces become important. Unfortunately, the upper surface, leading to a $^2\Pi$ and a $^2\Sigma$ fragment, has not -- to the best of my knowledge -- been characterised.[15] Thus, it is not clear at what distance the difference between the two repulsive potentials becomes small. However, since the equilibrium bond distance in the $^2\Sigma$ state is very close to that in the $^2\Pi$ state,[6,16] the L parameter in the repulsive term should be similar for both surfaces. In this case, an estimate of 4Å for the separation at which the long-range forces become the dominant interaction is probably adequate.

We can express the long-range interaction of the two fragments, oriented as shown in the diagram, by the expression:[14]

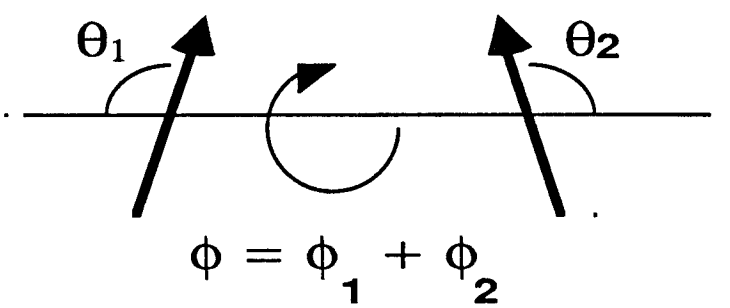

$$
\begin{aligned}
V = \; & \mu_1\mu_2 R^{-3}(2\cos\theta_1\cos\theta_2+\sin\theta_1\sin\theta_2\cos\phi) \\
& + 3/2\ \mu_1\Theta_2 R^{-4}[\cos\theta_1(3\cos^2\theta_2-1)+2\sin\theta_1\sin\theta_2\cos\theta_2\cos\phi] \\
& + 3/2\ \mu_2\Theta_1 R^{-4}[\cos\theta_2(3\cos^2\theta_1-1)+2\sin\theta_1\sin\theta_2\cos\theta_1\cos\phi] \\
& + 3/4\ \Theta_1\Theta_2 R^{-5}(1-5\ \cos^2\theta_1-5\cos^2\theta_2+17\cos^2\theta_1\cos^2\theta_2 \\
& \quad + 2\sin^2\theta_1\sin^2\theta_2\cos^2\phi\ +16\sin\theta_1\cos\theta_1\sin\theta_2\cos\theta_2\cos\phi) \\
& + \ldots
\end{aligned}
$$

Since both the sign and magnitude of this potential is highly dependent

upon the angles θ_1 and θ_2, the shift from nascent absorption in this regime is going to be heavily dependent upon the exact nature of the dissociative mechanics. If the fragments tend to be produced with a specific orientation with respect to each other, then this will manifest itself in the nature of the off-resonance absorption. Of course, this effect may be masked by the absorption from the exponentially repulsive part of the dissociative surface; however, it is likely that the transition moment for absorption in this region is larger than that closer in. In this regime, the transition moment should be that of the free radical, since the interaction does not greatly effect the wavefunctions. However, when the fragment separation is much smaller, the transition moment should be more typical of closed-shell molecular transition moments, which are generally several orders of magnitude smaller.[17] This will make the probability for absorption much greater by fragments at these larger separations.

The Interaction of Highly Aligned Fragments

In an attempt to understand the effect of the fragment alignment upon the off-resonant absorption of the fragment, we will make a rather draconian assumption about the hydroxyl fragments. We know that the fragments have a tendency to align their angular momenta along the recoil velocity; we will assume that the projection of the angular momentum onto the velocity vector is as large as possible. In other words, by quantizing the angular momentum along the recoil velocity, we will

assume that the fragment angular wavefunction is Y_j^j (in fact, it is just as likely to be Y_{-j}^j, but, since only |m| will affect the calculations, it will be simpler to confine the wavefunction to Y_j^j).

For fixed fragment separation R, we want to evaluate $\langle j_1 m_1 j_2 m_2 | V | j_1 m_1 j_2 m_2 \rangle$ for the long-range interaction V given previously. Inversion of coordinates takes (θ_i,ϕ_i) to $(\Pi-\theta_i,\Pi+\phi_i)$. Inverting the coordinates of either fragment 1 or fragment 2 changes the sign of the first three terms of the long-range potential -- the dipole-dipole and both mixed dipole-quadrupole terms. These terms will then average to zero over all space (since the weighting function $\Psi^*\Psi$ is even). Thus, the first non-zero term in the average is the quadrupole-quadrupole interaction. By expanding this term in terms of the spherical harmonic vectors, we will greatly simplify its evaluation.[18] In fact, it can easily be found that:

$$
\begin{aligned}
V_{\Theta-\Theta} = {} & 1 - 5/3\,[(16\pi/5)^{1/2}\, Y_0^2(1) + 1] - 5/3\,[(16\pi/5)^{1/2}\, Y_0^2(2) + 1] \\
& + 17/9\,[(16\pi/5)^{1/2}\, Y_0^2(1) + 1]\,[(16\pi/5)^{1/2}\, Y_0^2(2) + 1] \\
& + 1/9\,[2 - (16\pi/5)^{1/2}\, Y_0^2(1)]\,[2 - (16\pi/5)^{1/2}\, Y_0^2(2)\,] \\
& + 8\pi/15\,\{[(Y_2^2+Y_{-2}^2)(1)][(Y_2^2+Y_{-2}^2)(2)] \\
& \qquad + [(Y_2^2-Y_{-2}^2)(1)][(Y_2^2-Y_{-2}^2)(2)]\} \\
& + 32\pi/5\,\{[(Y_{-1}^2-Y_1^2)(1)][(Y_{-1}^2-Y_1^2)(2)] \\
& \qquad + [(Y_{-1}^2+Y_1^2)(1)][(Y_{-1}^2+Y_1^2)(2)]\}
\end{aligned}
$$

where $Y_m^j(i) = Y_m^j(\theta_i,\phi_i)$

We will now make use of the spherical harmonic addition theorem:[19]

$$\iint Y_m^j Y_n^k Y_o^l = [(2j+1)(2k+1)(2l+1)/4\pi] \begin{pmatrix} j & k & l \\ 0 & 0 & 0 \end{pmatrix} \begin{pmatrix} j & k & l \\ m & n & o \end{pmatrix}$$

where $\begin{pmatrix} j & k & l \\ 0 & 0 & 0 \end{pmatrix}$ and $\begin{pmatrix} j & k & l \\ m & n & o \end{pmatrix}$ are Wigner 3-j symbols. Using this relation we find that:

$$\iint (Y_j^j)^* Y_m^2 Y_j^j = (-)^j \iint Y_{-j}^j Y_m^j Y_j^j$$
$$= (-)^j [5(2j+1)^2/4\pi] \begin{pmatrix} j & 2 & j \\ 0 & 0 & 0 \end{pmatrix} \begin{pmatrix} j & 2 & j \\ -j & m & j \end{pmatrix}$$

These 3-j symbols have been evaluated[19] and:

$$\begin{pmatrix} j & 2 & j \\ 0 & 0 & 0 \end{pmatrix} = (-)^{j+1} \; 2j(j+1)/[(2j+3)(2j+2)(2j+1)2j(2j-1)]^{1/2}$$

$$\begin{pmatrix} j & 2 & j \\ -j & m & j \end{pmatrix} = \delta_{m,0} \times 2[3j^2 - j(j+1)]/[(2j+3)(2j+2)(2j+1)2j(2j-1)]^{1/2}$$

These give $\langle Y_m^j \rangle = \delta_{m,0} \times -(5/4\pi)^{1/2} j/(2j+3)$ and, ultimately:

$$\langle V \rangle = 6 \Theta_1 \Theta_2 R^{-5} j_1 j_2/(2j_1+3)(2j_2+3).$$

Chu and coworkers[16] have estimated the quadrupole moment of OH in both the $^2\Pi$ and $^2\Sigma$ states as a function of O-H distance. For a vertical transition, we will want to know the quadrupole moments of both states at the equilibrium geometry of the lower, which is R_e = 1.84 bohr.[16] At this bond length, $\Theta = 1.82 \times 10^{-26}$ esu-cm^2 for the lower state and $\Theta = 4.05 \times 10^{-26}$ esu-cm^2 for the upper. For the transition $\Delta j=0$ and $\Delta m=0$, the perturbation to the energy is:

$$\Delta h\upsilon = (1.2 \times 10^5 \text{ cm}^{-1}\text{-Å}^5) R^{-5} j_1 j_2/(2j_1+3)(2j_2+3)$$

For large j, this gives, for instance, a perturbation of $29cm^{-1}$ at a separation of 4Å and $3.8cm^{-1}$ at 6Å. Thus, for large j, we would estimate an off-resonant absorption spectrum that began several angstroms to the blue. Notice, however, that as j becomes small, this drops off quite rapidly. For $j_1 = 1$, we would expect a shift 1/5 as large.

Essentially, what we have shown is that dissociation dynamics which align fragments in this manner, create fragments which have a blue shifted spectrum. However, since the amount that the angular momentum vector can be aligned with the velocity vector decreases with decreasing J, this blue-shifting tends to be averaged out for those hydroxyls with small angular momenta. We recognize that our confinement of the wavefunction to Y^j_j is extreme; however, if our model is qualitatively correct, then we should see a spectrum which shows similar red-shifted features for all J_{OH} but whose blue-shifted features decrease as J_{OH} decreases.

By way of contrast, we can calculate the interaction of a fragment whose angular is aligned perpendicular to its velocity with one aligned as above. This may be relevant, for instance, in the case of probing fragments with small angular momenta. In this case, a substantial portion of their angular momentum may have been produced by in plane bending or some other mechanism that runs counter to the predominant

one. Since this fragment with small J will be most likely paired with one with high J,[12] the alignments of the two fragments in this case should be opposite.

In a similar fashion to the last example, we want to calculate $\langle j_1 0 j_2 j_2 | V | j_1 0 j_2 j_2 \rangle$. It can be shown that:

$$\langle j_1 0 | Y_m^2 | j_1 0 \rangle = \delta_{m,0} \times (5/4\pi)^{1/2} \, j_1(j_1+1)/(2j_1+3)(2j_1-1)$$

and, finally, $\langle V \rangle = \Theta_1 \Theta_2 R^{-5} [-64 j_1^2 j_2 - 64 j_1 j_2 + 30 j_2 + 8 j_1^2 + 8 j_1 + 39] \times [4(2j_1+3)\,(2j_1-1)\,(2j_2+3)]^{-1}$

This expression differs in two regards from the one derived above. First, the perturbation has the opposite sign. Thus, for OH, whose excited state quadrupole moment is larger than its ground-state one, the shift will be to the red. Secondly, as j_1 increases, the shift decreases -- the exact opposite effect of the case above.

Future Work

As we have tried to show, the long-range potential should have a substantial (on the order of 5 - 10 cm^{-1}) effect upon absorption of fragments on dissociative surfaces. More significantly, the exact nature of this effect is very dependent upon the dynamics of the dissociation, in particular, upon the preferred relative orientation of the fragments. Given the combination of short pulses and narrow spectral width available in the picosecond domain, we feel this technique will prove to be a powerful tool

for the investigation of fast photodissociations. To this end, we have taken spectra, as oppossed to the transients shown in the figures, in order to more clearly observe the spectral features of the absorption. In this case, we scanned the probe wavelength and measured the resulting emission as a function of wavelength (instead of time). By taking a series of spectra, each with identical ranges, but with the probe pulse antecedent, simultaneous, and subsequent to the pump, we hope to remove the effects of backround (such as scattering of the probe) and nascent absorption. We are currently developing techniques to disentangle the effects of pulse width and on-resonant absorption from the off-resonant features. However, the off-resonant absorption does seem asymmetric, with sizable absorption to the blue and a long red tail. We are confident that with more sophisticated data-processing we will be able to quantify the affects mentioned above.

REFERENCES

(1) a) J. C. Polanyi and R. J. Wolf *J. Chem. Phys.* **1981**, 75, 5951.
b) H. J. Foth; J. C. Polanyi; and H. H. Telle *J. Phys. Chem.* **1982**, 86, 5027.
c) H. R. Mayne; R. A. Poirer; and J. C. Polanyi *J. Chem. Phys.* **1984**, 80, 4025.
d) H. R. Mayne; J. C. Polanyi; N. Sathyamurthy; and S. Raynor *J. Phys. Chem.* **1984**, 88, 4064.
e) B. A. Collins, *et. al.* private communication.

(2) a) M. Dantus; M. J. Rosker; and A. H. Zewail *J. Chem. Phys.* **1987**, 87, 2395.
b) L. R. Khundkar and A. H. Zewail *Chem. Phys. Lett.* **1987**, 142, 427.
c) R. Bersohn and A. H. Zewail *Ber. Bunsenges Phys. Chem.* submitted for publication.

(3) See, for example, reference 14 of reference 2a.

(4) a) S. Klee; K. H. Gericke; and F. J. Comes *J. Chem. Phys.* **1986**, 85, 40.
b) K. H. Gericke; S. Klee, F. J. Comes; and R. N. Dixon *J. Chem. Phys.* **1986**, 85, 4463.

(5) a) L. R. Khundkar; J. L. Knee; and A. H. Zewail *J. Chem. Phys.* **1987**, 87, 77.
b) N. F. Scherer and A. H. Zewail *J. Chem. Phys.* **1987**, 87, 97.
c) J. L. Knee; L. R. Khundkar; and A. H. Zewail *J. Chem. Phys.* **1987**, 87, 115.

(6) J. A. Coxon; K. V. L. N. Sastry; J. A. Austin; and D. H. Levy *Can. J. Chem.* **1979**, 57, 619.

(7) a) P. A. Giguerre *J. Chem. Phys.* **1959**, 30, 322.
b) D. L. Bauch; *et. al. J. Phys. Chem. Ref. Data* **1980**, 9, 295.

(8) a) M. P. Docker; A. Hodgson; and J. P. Simons *Chem. Phys. Lett.* **1986**, 128, 264.
b) M. P. Docker; A. Hodgson; and J. P. Simons *Faraday Discuss. Chem. Soc.* **1986**, 82, 25.
c) J. P. Simons *J. Phys. Chem.* **1987**, 91, 5378.

(9) a) G. E. Hall, *et. al. Faraday Discuss. Chem. Soc.* **1986**, 82, 13.
b) R. N. Dixon *J. Chem. Phys.* **1986**, 85, 1866.
c) P. L. Houston *J. Phys. Chem.* **1987**, 91, 5388.

(10) S. Yang and R. Bersohn *J. Chem. Phys.* **1974**, 61, 4400. and references contained therein.

(11) See, for example, references 4b and 8b.

(12) R. Bersohn and M. Shapiro *J. Chem. Phys.* **1986**, 85, 1396.

(13) a) H. Margenau *Rev. Modrn. Phys.* **1939**, 11, 1.
b) Krishnaji and V. Prakash *Rev. Modrn. Phys.* **1966**, 38, 690.

(14) a) A. D. Buckingham *Quart. Rev.* **1959**, 13, 189.
b) A. D. Buckingham *Discuss. Faraday Soc.* **1965**, 40, 232.
c) A. D. Buckingham *Adv. Chem. Phys.* **1967**, XII, 107.

(15) See, however, H. Golzenleuchter; K. H. Gericke; F. J Comes; and P. F. Linde *Chem. Phys.* **1984**, 89, 93. and reference 21 therein.

(16) S. I. Chu; M. Yoshimine; and B. Liu *J. Chem. Phys.* **1974**, 61, 5389.

(17) Gerhard Herzberg "The Spectra and Structures of Simple Free Radicals" Cornell Univ. Press; Ithaca, N.Y.; 1971.

(18) See, for example, U. Fano and G. Racah "Irreducible Tensorial Sets" Academic Press, New York, 1959.

(19) See, for example, A. R. Edmonds "Angular Momentum in Quantum Mechanics; 2nd Ed." Princeton Univ. Press; Princeton, N.J., 1960.

Figure Caption

Figure 1: a) Each separate line is a transient showing OH LIF signal versus delay time in ps. The marked ordinate refers to the energy of the OH probe pulse relative to the $Q_1(1)$ transition in cm^{-1}.

b) A single transient taken with the probe laser $3cm^{-1}$ to the blue.

Figure 2a

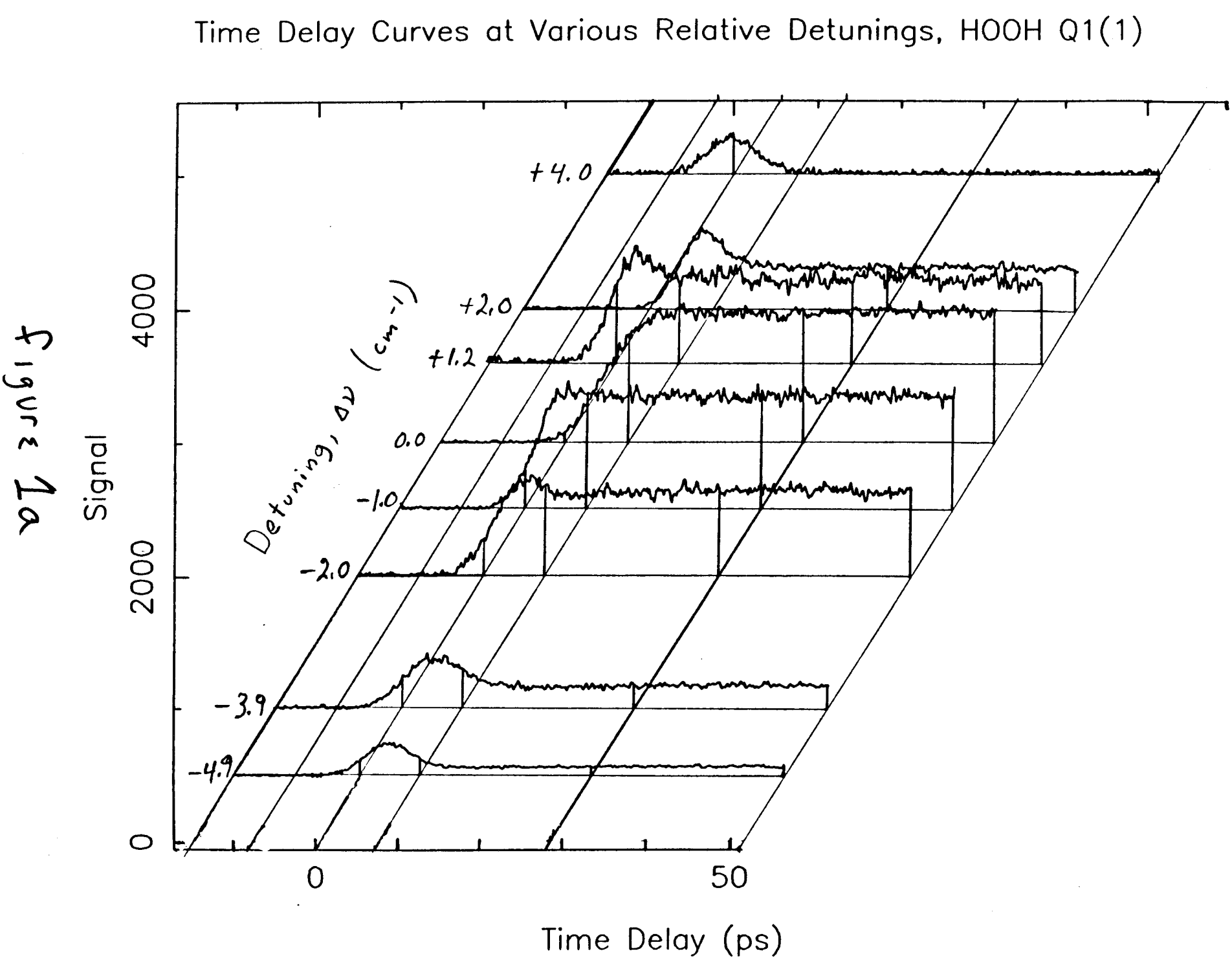
Time Delay Curves at Various Relative Detunings, HOOH Q1(1)
Signal
0
2000
4000
Detuning, Δν (cm⁻¹)
+4.0
+2.0
+1.2
0.0
-1.0
-2.0
-3.9
-4.9
0
50
Time Delay (ps)

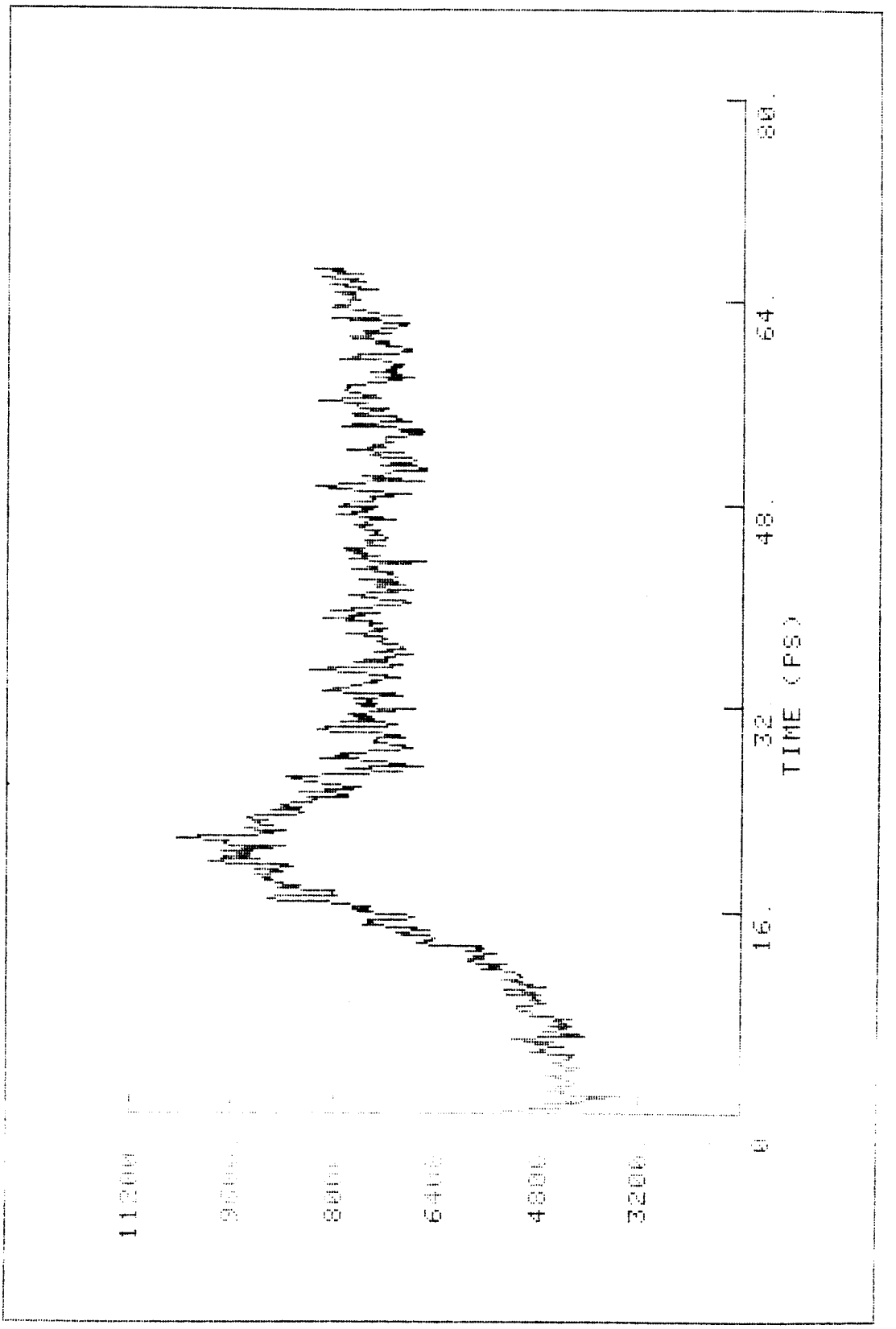

Figure 1b